


# Temporally and spatially dynamic redox conditions on an upwelling margin: The impact on coupled sedimentary Mo and U isotope systematics, and implications for the Mo-U paleoredox proxy

## Journal Article

### Author(s):

He, Zhiwei; Clarkson, Matthew O.; Andersen, Morten B.; [Archer, Corey](#) ; Sweere, Tim C.; Kraal, Peter; Guthauser, Alex; Huang, Fang; Vance, Derek

### Publication date:

2021-09-15

### Permanent link:

<https://doi.org/10.3929/ethz-b-000497228>

### Rights / license:

[Creative Commons Attribution 4.0 International](#)

### Originally published in:

Geochimica et Cosmochimica Acta 309, <https://doi.org/10.1016/j.gca.2021.06.024>

### Funding acknowledgement:

795722 - How does the Earth stop global warming? Using metal isotopes to understand climate recovery processes (EC)  
834236 - Nutrients in anoxic oceans – Trace metals in modern and ancient environments (EC)





# Temporally and spatially dynamic redox conditions on an upwelling margin: The impact on coupled sedimentary Mo and U isotope systematics, and implications for the Mo-U paleoredox proxy

Zhiwei He<sup>a,b,c,\*</sup>, M.O. Clarkson<sup>b</sup>, M.B. Andersen<sup>d</sup>, Corey Archer<sup>b</sup>, Tim C. Sweere<sup>b</sup>, Peter Kraal<sup>e</sup>, Alex Guthausen<sup>b</sup>, Fang Huang<sup>c,f</sup>, Derek Vance<sup>b,\*</sup>

<sup>a</sup> State Key Laboratory of Marine Geology, Tongji University, Shanghai 200092, China

<sup>b</sup> Institute of Geochemistry and Petrology, Department of Earth Sciences, ETH Zürich, Clausiusstrasse 25, Zürich 8092, Switzerland

<sup>c</sup> CAS Key Laboratory of Crust-Mantle Materials and Environments, School of Earth and Space Sciences, University of Science and Technology of China, Hefei 230026, Anhui, China

<sup>d</sup> School of Earth & Ocean Sciences, Cardiff University, Park Place, Cardiff CF10 3AT, United Kingdom

<sup>e</sup> Royal Netherlands Institute for Sea Research, Department of Ocean Systems, Landsdiep 4, 1797SZ Den Hoorn, The Netherlands

<sup>f</sup> CAS Center for Excellence in Comparative Planetology, Hefei 230026, Anhui, China

Received 23 June 2020; accepted in revised form 17 June 2021; Available online 24 June 2021

## Abstract

The abundances and isotope compositions of molybdenum (Mo) and uranium (U) in ancient sediments are promising tracers of the redox state of the past ocean, whose basis lies in the environmentally dependent Mo and U isotope signatures in modern oceanic settings. Despite their dominance in oceanic budgets, the controls on the Mo-U systematics of upwelling margin sediments remain to be fully understood. Here we present a comprehensive sediment-porewater Mo and U isotope study in the Benguela upwelling system off Namibia, including the first dataset incorporating coupled Mo-U abundance and isotope analysis of both solid authigenic phases and porewaters.

The investigated stations represent shelf-to-slope settings, which lie on the upper edge, within and below the oxygen minimum zone (OMZ) of the South Atlantic. The sediments across all stations share similar characteristics: both Mo and U show increasing authigenic enrichment with depth, coupled to an overall decrease in  $\delta^{98}\text{Mo}_{\text{auth}}$  (from  $\sim 2.0\text{‰}$  to  $1.3\text{‰}$  and from  $\sim 2.0\text{‰}$  to  $0.3\text{‰}$ ) and increase in  $\delta^{238}\text{U}_{\text{auth}}$  (from  $-0.18\text{‰}$  to  $0.05\text{‰}$  and from  $-0.34\text{‰}$  to  $-0.21\text{‰}$ ). Nevertheless, the extents of Mo and U enrichment and associated isotopic fractionations display spatial variability across the OMZ, reflecting variations in local sedimentary redox conditions. Porewater Mo and U concentration patterns are more complex, exhibiting peaks in Mo and U abundance well in excess of seawater (up to 8 times seawater for Mo) associated with correlated shifts in isotope composition. As a result, porewaters exhibit a wide range in isotope compositions, between  $0.90\text{‰}$  and  $2.79\text{‰}$  for  $\delta^{98}\text{Mo}$  and between  $-1.74\text{‰}$  and  $0.26\text{‰}$  for  $\delta^{238}\text{U}$ .

Porewater gradients at the time of sampling are inconsistent with diffusion downwards across the sediment-seawater interface as a means of enrichment of the sediment-porewater system. Though these sampled conditions may represent only a snapshot, so that periodically more reducing conditions could lead to concentration gradients that do permit downward diffusion, the data are also readily explained by addition of Mo and U to the sediment-porewater system in particulate form, also under more reducing conditions than at the time of sampling. For example, sequestration of Mo and U to particulate matter

\* Corresponding authors at: Institute of Geochemistry and Petrology, Department of Earth Sciences, ETH Zürich, Clausiusstrasse 25, Zürich 8092, Switzerland (Z. He).

E-mail addresses: [hezww@tongji.edu.cn](mailto:hezww@tongji.edu.cn) (Z. He), [derek.vance@erdw.ethz.ch](mailto:derek.vance@erdw.ethz.ch) (D. Vance).

as a result of the presence of intermittent sulfide, either in bottom water or in porewater right at the sediment–water interface, explains much of the geochemical and isotope data.

The data thus suggest that the early diagenetic enrichment of Mo and U in sediments of upwelling margins is strongly governed by temporal redox fluctuations. Early diagenesis under these dynamic redox conditions on the Namibian upwelling margin are strongly reflected in Mo–U co-variation patterns, as well as anti-correlations between authigenic  $\delta^{98}\text{Mo}$  and  $\delta^{238}\text{U}$  in sediments. Overall, our new data demonstrate that early diagenetic processes on open-marine continental margins reproduce patterns previously observed for coupled Mo–U isotope systematics in restricted and semi-restricted basins, but via a different set of processes and with important implications for the use of such a coupled approach in the study of ancient marine anoxia.

© 2021 The Author(s). Published by Elsevier Ltd. This is an open access article under the CC BY license (<http://creativecommons.org/licenses/by/4.0/>).

**Keywords:** Mo isotopes; U isotopes; Porewater; Continental margin sediments; OMZ

## 1. INTRODUCTION

The sedimentary record of molybdenum (Mo) and uranium (U) abundances and their isotope compositions are widely used to investigate past global marine redox conditions (e.g., Kendall et al., 2011; Azrieli-Tal et al., 2014; Chen et al., 2015; Cheng et al., 2016; Clarkson et al., 2018; Tostevin et al., 2019; Zhang et al., 2020). Many published studies have shown that Mo and U isotope systematics can provide clues to the intensity and timing of both oxygenation and deoxygenation of the past atmosphere–ocean system through Earth history (see recent reviews by Andersen et al., 2017; Kendall et al., 2017). The strength of Mo and U as paleoredox proxies results from their redox-dependent scavenging and isotope fractionation mechanisms (e.g., Neubert et al., 2008; Algeo and Tribouillard, 2009; Andersen et al., 2014; Noordmann et al., 2015; Dickson, 2017; Rolison et al., 2017).

In the modern well-oxygenated oceans, the dominant oxidized hexavalent species of Mo and U (as soluble molybdate  $\text{MoO}_4^{2-}$  and uranyl carbonate complexes  $\text{UO}_2(\text{CO}_3)_3^{4-}$ ) are rather inert, resulting in conservative behavior and nearly uniform concentrations (~110 nM and ~13.4 nM at a salinity of 35, respectively) (Collier, 1985; Tribouillard et al., 2006), homogenous  $^{98}\text{Mo}/^{95}\text{Mo}$  and  $^{238}\text{U}/^{235}\text{U}$  (Barling et al., 2001; Siebert et al., 2003; Stirling et al., 2007; Weyer et al., 2008; Andersen et al., 2010; Nakagawa et al., 2012; Tissot and Dauphas, 2015), and long oceanic residence times (~400–500 kyr) relative to the deep ocean renewal time of ~1 kyr (Dunk et al., 2002; Miller et al., 2011). In contrast, under reducing conditions, both elements become non-conservative and enriched in the sediments (Morford and Emerson, 1999).

Despite these broad similarities, Mo and U show differences in their specific removal pathways and associated isotope fractionations. In oxidizing marine environments, the output fluxes of Mo from seawater are governed by the adsorption of Mo onto Mn- and Fe-oxyhydroxide minerals, which are fractionated from seawater by  $-0.8\text{‰}$  to  $-3\text{‰}$  (Siebert et al., 2003; Barling and Anbar, 2004; Wasylenki et al., 2008; Goldberg et al., 2009). This light output is the main driver of the heavy isotopic composition of Mo in the modern dissolved pool, with  $\delta^{98}\text{Mo}$  of  $2.34\text{‰}$  relative to the riverine input of  $0.7\text{‰}$  (Siebert et al., 2003; Archer and Vance, 2008; Nakagawa et al., 2012). On the

other hand, Mo is rapidly removed in sulfidic environments, due to the transformation of soluble molybdate to particle-reactive thiomolybdates ( $\text{MoO}_{4-x}\text{S}_x^{2-}$ ,  $1 < x < 4$ ) in the water column and below the sediment–water interface (Helz et al., 1996; Erickson and Helz, 2000). In strongly euxinic settings, where the aqueous  $\text{H}_2\text{S}$  concentration exceeds  $11 \mu\text{M}$ , the conversion of molybdate to tetrathiomolybdate ( $\text{MoS}_4^{2-}$ ) is nearly complete and Mo can be quantitatively scavenged into sulfidic sediments (Erickson and Helz, 2000). Sediments in these settings (for example, in the Black Sea) can ultimately evolve to isotope compositions that approach the seawater source (Nägler et al., 2005; Neubert et al., 2008).

In contrast to Mo, U occurs as the chemically labile U (VI) in the water column, even under highly euxinic conditions, and its reduction and removal is thought to primarily occur within the sediment–porewater system (Anderson et al., 1989). In terms of  $^{238}\text{U}/^{235}\text{U}$ , uranium isotopes are also uniformly distributed in the dissolved pool of the modern open ocean, with a mean  $\delta^{238}\text{U}$  of  $-0.39 \pm 0.01\text{‰}$  (2SD) that is slightly lower than that ( $-0.26\text{‰}$ ) of the riverine input (Stirling et al., 2007; Weyer et al., 2008; Tissot and Dauphas, 2015; Andersen et al., 2016). This difference between riverine inputs and the open ocean isotopic composition is largely driven by the removal of U into anoxic sinks (Andersen et al., 2016), where  $^{238}\text{U}$  is preferentially enriched in reduced U(IV) solid phases, relative to  $^{235}\text{U}$ , due to the nuclear field shift effect (Schauble, 2007; Abe et al., 2008). Other U removal processes besides U reduction, including oxic adsorption of U onto organic matter (OM), pelagic carbonates, and oxyhydroxides (Brennecke et al., 2011; Holmden et al., 2015; Hinojosa et al., 2016; Clarkson et al., 2020), account for only a minor proportion of the total oceanic removal flux for U (Andersen et al., 2017).

Much of our detailed understanding of the mechanisms for, and isotope fractionations associated with, removal of Mo and U derives from studies of marginal marine basins that are often euxinic, i.e., that feature substantial dissolved sulfide in the water column (e.g., Neubert et al., 2008; Andersen et al., 2014; Noordmann et al., 2015; Rolison et al., 2017; Bura-Nakić et al., 2018). In particular, recent studies have identified a general inverse correlation between the Mo and U isotope compositions of sediments in euxinic basins, implying a similar response of isotope fractionation

to the efficiency of Mo and U removal into sediments (e.g., Andersen et al., 2018, 2020; Bura-Nakić et al., 2018; Brüske et al., 2020; Kendall et al., 2020; Lu et al., 2020). These findings have highlighted the potential in the use of the paired Mo-U isotopes as a paleoredox proxy (Andersen et al., 2020; Brüske et al., 2020).

However, it has become increasingly clear that such marginal euxinic basins are of rather minor importance for the overall oceanic budgets of Mo and U (see reviews in Andersen et al., 2017; Kendall et al., 2017), and that open marine, upwelling margins are much more important – in the case of Mo they are the sites of burial of more than half of oceanic Mo. The sediments of such settings feature a wide range of  $\delta^{98}\text{Mo}$  that are isotopically intermediate between the light oxic sink and modern seawater (e.g., Siebert et al., 2006; Poulson Brucker et al., 2009; Dickson et al., 2014; Scholz et al., 2017; Eroglu et al., 2020). The explanations for these variable Mo isotope fractionations are complicated by multiple Mo fixation mechanisms, involving non-quantitative Mo scavenging by Fe- and Mn-oxides, or by conversion of Mo to thiomolybdates under low  $\text{H}_2\text{S}$  concentrations. Moreover, reported  $\delta^{238}\text{U}$  for the sediments also span a wide range, between  $-0.62\text{‰}$  and  $0.20\text{‰}$ , reflecting U isotope fractionation during early diagenesis and post-depositional remobilization (Weyer et al., 2008; Andersen et al., 2016; Abshire et al., 2020a). Consequently, the Mo and U isotope systematics in open-marine continental margin sediments are subject to complex and temporally variable redox conditions.

The full potential of coupled Mo and U isotopes as a paleoredox proxy can only be realized through more detailed calibration work undertaken in such open-marine settings. In this study, we present a comprehensive Mo and U isotope investigation of the sediment-porewater system at one of the world's most intense upwelling areas: the Namibian margin. We present, for the first time in such a setting, coupled Mo and U concentrations and isotope compositions of both sediments and porewaters. We investigate the influence of the temporally and spatially dynamic redox conditions characteristic of such upwelling settings on Mo and U cycling and their isotope fractionations, an essential prerequisite for the robust interpretation of sedimentary records of  $\delta^{98}\text{Mo}$  and  $\delta^{238}\text{U}$ . Finally, we take the opportunity to assess, in the context of the new data, the global application of coupled Mo-U isotopes as a paleoredox proxy for open-marine anoxia.

## 2. STUDY AREA

The Namibian margin (see setting of sites studied here in Figs. 1 and 2) occupies one of the world's most productive marine ecosystems, with significant coastal upwelling associated with the Benguela Upwelling System (BUS; Nelson and Hutchings, 1983; Shannon and Nelson, 1996). The BUS forms the southern part of the eastern boundary current system of the south Atlantic (Stramma and England, 1999), which comprises the poleward flowing Benguela Undercurrent (BUC) and the equatorward flowing Benguela Current (BC; Fig. 1). Overall, the Benguela Current consists of an oceanic (Benguela Oceanic Current, BOC)

and a coastal (Benguela Coastal Current, BCC) branch (Fig. 1), while the BUC is regarded as a poleward continuation of the Angola Current (AC) below the thermocline (Mohrholz et al., 2008). The BCC and BUC systems converge in the Angola-Benguela Frontal Zone (ABFZ) at  $14\text{--}16^\circ\text{S}$ , marking the northern boundary of the BUS. The upwelling of nutrient-rich subsurface South Atlantic Central Water (SACW), forced by the persistent alongshore southeasterly wind, has resulted in a number of local upwelling cells along the entire coast of the Benguela area between  $16^\circ\text{S}$  and  $34^\circ\text{S}$  (Shannon, 1985).

The perennial Lüderitz cell at  $\sim 26.5^\circ\text{S}$  is the strongest upwelling cell of the BUS area and splits the system into northern and southern regions, with distinct characteristics (Shannon and Nelson, 1996). The northern Benguela is characterized by perennial alongshore winds and upwelling along the coast, where oxygen-depleted SACW is transported southward by the poleward BUC. Under the dominance of SACW complete loss of oxygen can occur in a stagnant bottom water layer, which is conducive to the development of an oxygen minimum zone (OMZ) above the Namibian shelf and upper slope (Weeks et al., 2002; Monteiro et al., 2006; Mohrholz et al., 2008; Nagel et al., 2013). In the south, by contrast, the trade winds are seasonal and upwelling peaks during austral spring and summer, where upwelling entrains well-oxygenated Eastern South Atlantic Central Water (ESACW) into the offshore Ekman drift (Mohrholz et al., 2008).

Previous studies of the Namibian margin have emphasized the temporal heterogeneity of the OMZ due to variations in upwelling strength on seasonal and longer timescales (e.g., Borchers et al., 2005; Böning et al., 2020). Large parts of the BUS are classified as being almost permanently suboxic, and the near-shore and shelf bottom waters are periodically anoxic (Borchers et al., 2005). Parts of the BUS are also characterized by transient buildups of  $\text{H}_2\text{S}$  in sediment porewaters during periods of intense upwelling and productivity (Weeks et al., 2002, 2004; Brüchert et al., 2003, 2006, 2009; Emeis et al., 2004; Ohde and Dadou, 2018), and episodic  $\text{H}_2\text{S}$  concentrations exceeding  $100\ \mu\text{M}$  in bottom water (Brüchert et al., 2006; Currie et al., 2018). Catastrophic manifestations of bottom water sulfide events have been attributed to the eruptive flux of methane carrying  $\text{H}_2\text{S}$  from gas-charged shelf sediments (Weeks et al., 2002, 2004; Emeis et al., 2004). Though Brüchert et al. (2006) suggest that these may be restricted to the region between  $23^\circ\text{S}$  and  $24^\circ\text{S}$ , well to the north of the sites studied here ( $26^\circ\text{S}$ ), at water depths of  $<100\ \text{m}$ , these authors also acknowledge that data coverage is too thin to rule out undetected gas-filled areas within sediment at other localities between  $22^\circ\text{S}$  and  $27^\circ\text{S}$ .

Brüchert et al. (2006), in fact, also note that findings of significant bottom-water  $\text{H}_2\text{S}$  occur over a much larger area, including as far south as  $26.5^\circ\text{S}$  (Weeks et al., 2002, 2004). At these latitudes, encompassing the sites studied here, Brüchert et al., (2006) suggest that processes other than ebullition and gas eruption lead to the periodically observed water column sulfide, and that sulfate reduction rates as well as low sedimentary reactive Fe contents lead to significant diffusive fluxes of  $\text{H}_2\text{S}$  from the sediment to

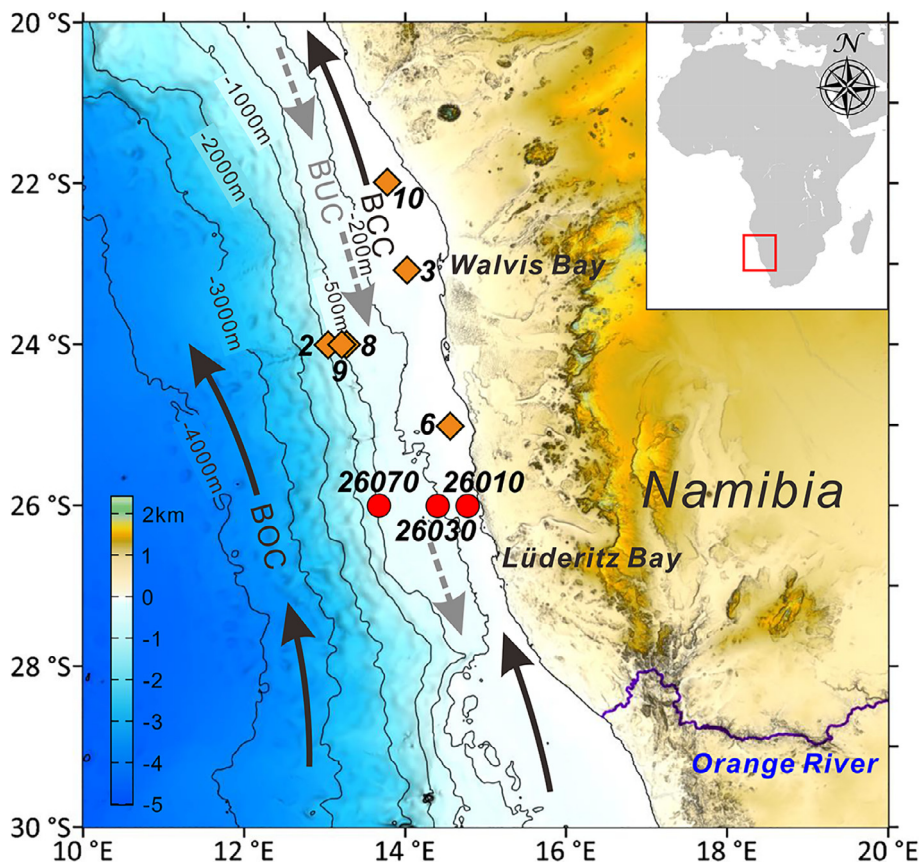


Fig. 1. Bathymetric map of the study area off Namibia showing sampling locations during cruises on Namibia's R/V MIRABILIS in April 2017 (red circles) and on cruise 64PE449 in February 2019 (orange diamonds). Schematic currents are modified from [Inthorn et al. \(2006a\)](#). The black arrows mark the main surface branches of the Benguela current system: BOC = Benguela Oceanic Current, BCC = Benguela Coastal Current. The dashed grey arrows mark the poleward undercurrent over the outer shelf: BUC = Benguela Under-Current. (For interpretation of the references to colour in this figure legend, the reader is referred to the web version of this article.)

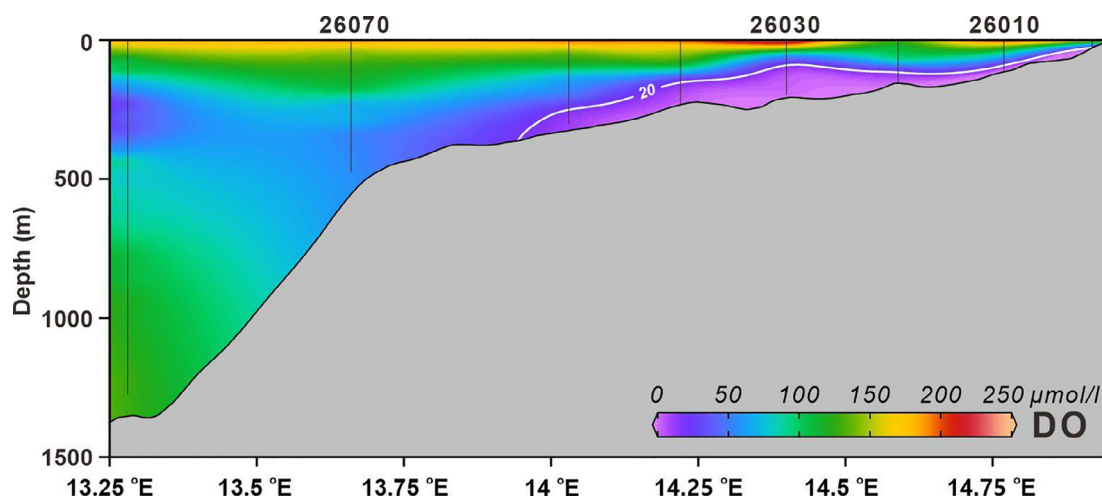


Fig. 2. Water column redox conditions across the Namibian continental margin at 26°S during cruises on Namibia's R/V MIRABILIS in April 2017. The vertical lines mark the locations of CTD stations. The locations of the studied sediment cores (stations 26010, 26030, and 26070) are marked at the top, which lie at the upper edge, within and below the OMZ, respectively. Seabed topographic imagery was reproduced from the GEBCO\_2014 Grid (<https://www.gebco.net/>).

bottom water. Whatever the origin, remote-sensing observations (Weeks et al., 2002, 2004) demonstrate that water column sulfide is an intermittent feature of the Namibian shelf at the locations sampled here.

The BUS off Namibia also hosts a variety of sedimentary environments from near-shore mud belt, through sandy shelf sediments, to fine-grained sediments in the low energy environment of the upper continental slope. The overall sedimentation rates are high, with estimates from  $\geq 100$  cm kyr<sup>-1</sup> on the shelf and between 5 and 17 cm kyr<sup>-1</sup> on the upper slope (Mollenhauer et al., 2002). The near-shore sediments, beneath the high productivity upwelling cell, contain a large fraction of organic-rich diatomaceous debris (Borchers et al., 2005), and form a very extensive mud belt that stretches over 700 km along-shore and is up to 100 km wide (Bremner, 1981). Sediments on the shelf are usually sandy and are interspersed with shell fragments and glauconite grains. In particular, the inner shelf surface sediments between 19°S and 27°S (Brüchert et al., 2006) feature high concentrations of H<sub>2</sub>S, with low concentrations of reactive iron in diatomaceous muds limiting precipitation of H<sub>2</sub>S as Fe mono-sulfide or pyrite (Borchers et al., 2005; Böning et al., 2020). Surface sediment concentrations of organic carbon (OC) are variable across the Namibian margin (Calvert and Price, 1983), and are barely diluted by terrigenous input due to the absence of perennial rivers (except for the Orange; Fig. 1). The sediments on the slope are often rich in clays and carbonate and do not show OC enrichment. The exception is a distinct depocenter at water depth of ~400–500 m between 24°S and 26.5°S, where OC as high as 9 wt% has been attributed to lateral redistribution from the shelf towards the slope by nepheloid layers (Inthorn et al., 2006a, 2006b).

### 3. METHODS

#### 3.1. Sampling and onboard analytics

The main comprehensive dataset, incorporating concentration and isotope analyses on both sediment and pore waters, derives from a transect along 26°S. Three sediment cores were retrieved during cruises on Namibia's R/V MIRABILIS in April 2017 as part of the Regional Graduate Network in Oceanography (RGNO) program. In addition, six more sediment cores were sampled in February 2019 (R/V Pelagia, cruise 64PE449), for porewater metal concentrations only, from the upwelling region north of 26°S. Bottom water metal concentrations were also provided for these latter sites. The geographical position and oxygen concentrations in the water column of all sampling stations are summarized in Table 1 and illustrated in Fig. 1. At the time of sampling of the set of cores along 26°S, CTD data indicated that the Namibian margin was overlain by an OMZ, with the core (O<sub>2</sub> < 20 μmol/L) ranging roughly from 100 to 300 m water depth (Fig. 2). Stations 26010, 26030, and 26070 lie at the upper edge, within and below the OMZ, respectively.

For the 26°S sites, sediment samples were retrieved using a multi-corer equipped with PVC tubes, one of which had

pre-drilled holes at cm resolution in order to facilitate porewater sampling. In the absence of an on-board anoxic sampling environment, cores were sampled immediately, i.e. completed within ~30 min, upon collection to minimize any oxidation of the porewaters. Prior to porewater extraction, bottom water was immediately drained through the hole above the sediment–water interface, and the pre-cleaned Rhizons were inserted at all intervals to allow simultaneous extraction and to minimize cross-contamination between intervals. Porewaters were then extracted *in-situ* using Rhizon samplers attached to syringes (Seeborg-Elverfeldt et al., 2005), directly inserted into the sediment samples. The extracted porewaters were then transferred to pre-cleaned 30 mL LDPE bottles (with each individual sample representing a volume between 4 and 17 mL; Table S1), and acidified to pH < 2 with concentrated trace metal grade nitric acid. Prior to sampling, porewater dissolved H<sub>2</sub>S concentrations were measured, *in-situ*, onboard the ship using a Unisense H<sub>2</sub>S microsensor. Before use the H<sub>2</sub>S sensor was calibrated against known concentrations of dissolved sodium sulfide. The detection limit is 0.3 μM H<sub>2</sub>S. Solid sediment from an adjacent core was sliced immediately upon recovery into 1–5 cm intervals. Sediments were then dried and stored for later processing. The multi-cores retrieved in February 2019 on cruise 64PE449 were processed on-board, in temperature-controlled laboratory containers at bottom-water temperatures. Sediments were sampled in an N<sub>2</sub>-filled glove bag, followed by centrifugation to separate the porewaters. The bottom- and -pore waters were filtered with a 0.45 μm PES filter and acidified to pH < 2 with Ultrapur HCl.

#### 3.2. Sample preparation and chemical characterization

Sediment and porewater samples were analyzed for elemental concentrations and isotope compositions in the clean labs at ETH Zürich. The porewater samples were weighed and then transferred to pre-cleaned Teflon beakers. An aliquot of each porewater sample was diluted x100 for the determination of elemental concentrations. For the sediments, approximately 50–100 mg of the powdered samples was weighed. The samples were digested on a hotplate with a 4:1 mixture of concentrated HF and HNO<sub>3</sub>, dried down to remove HF, refluxed in 6 N HCl to remove fluorides, and then re-dissolved in concentrated nitric acid with 10 vol.% concentrated H<sub>2</sub>O<sub>2</sub> to oxidise organic matter. Finally, the samples were brought up in 0.3 N nitric acid for elemental analysis.

Elemental concentrations were obtained using a Thermo-Fisher Element XR sector-field ICP-MS after the addition of indium internal standard. Accuracy and precision were assessed using two secondary multi-element standards: the National Research Council of Canada river standard SLRS5, and USGS shale standard SGR1. The concentrations obtained matched certified values to within 5–10% for the elements reported here. Total organic carbon (TOC) content of the sediments was measured using an Elemental Analyzer at ETH Zürich, after addition of dilute HCl to remove inorganic carbon. Repeat analyses and com-

Table 1  
Position, water depth, bottom water oxygen concentration, depositional location for stations on Namibian margin.

Station #	Latitude	Longitude	Water depth (m)	Bottom water oxygen ( $\mu\text{mol/L}$ ) <sup>a</sup>	Depositional location
Cruise in April, 2017					
26010	26° 00.007' S	14° 46.467' E	116	10.70 (109 m)	inner shelf
26030	26° 00.05' S	14° 24.44' E	198	2.34 (197 m)	middle shelf
26070	25° 59.986' S	13° 40.251' E	509	58.21 (476 m)	upper slope
Cruise in February, 2019					
6	25° 4.33' S	14° 35.77' E	100	3	inner shelf
10	21° 58.08' S	13° 47.56' E	103	3	inner shelf
3	23° 5.75' S	14° 7.68' E	136	20	inner shelf
8	23° 56.31' S	13° 17.96' E	324	44	middle shelf
9	23° 57.71' S	13° 13.57' E	407	65	shelf break
2	24° 1.58' S	13° 7.55' E	750	105	upper slope

<sup>a</sup> Bottom water oxygen concentrations were detected by CTD. The bracket numbers refer to the water depth for CTD measurements.

parison with certified standards indicate that the precision is  $\pm 0.2$  wt.% (2SD). The pyrite Fe ( $\text{Fe}_{\text{py}}$ ) content of the sediments was determined gravimetrically following precipitation of the liberated sulfide as  $\text{Ag}_2\text{S}$  by reacting with hot acidified  $\text{CrCl}_2$  solution (Canfield et al., 1986).

### 3.3. Molybdenum and uranium isotope analysis

Following concentration analysis, sediment sample aliquots containing a total of  $\sim 50$ – $500$  ng Mo and  $\sim 25$ – $100$  ng U were taken for isotopic analysis. The sediment samples were spiked with a  $^{97}\text{Mo}$ – $^{100}\text{Mo}$  double-spike (Archer and Vance, 2008), aiming for a 1:1 spike to sample ratio, and IRMM-3636  $^{233}\text{U}$ – $^{236}\text{U}$  double-spike (Richter et al., 2008), aiming for a 1:30  $^{236}\text{U}$  to  $^{238}\text{U}$  ratio. Porewater samples containing  $\sim 100$ – $600$  ng Mo and  $\sim 10$ – $100$  ng U were also spiked with the Mo and U double-spikes. After spiking, the porewater samples were dried down and re-dissolved in 7 N HCl. During this step, a large NaCl precipitate formed in porewater samples due to their high Na content. The supernatant was transferred into another pre-cleaned Teflon beaker. Yields obtained through comparison of the signal size from the isotope analysis with the Mo and U abundances defined by isotope dilution at the time of spiking indicate that the salt contained insignificant Mo and U. All spiked samples were then dried down and re-dissolved in 1 mL 1 N HCl in preparation for column chromatography.

Molybdenum and U were isolated from matrix elements using a home-made shrink-fit Teflon column containing  $\sim 0.2$  mL 50– $100$   $\mu\text{m}$  RE resin (Triskem Technologies), following a procedure modified from Bura-Nakić et al. (2018). Prior to sample loading, the RE resin was added to the columns, the resin was pre-cleaned using 2 mL of 0.2 N HCl, and pre-conditioned with 1 mL of 1 N HCl. Samples were then loaded in 1 mL 1 N HCl and the matrix was eluted with 4 mL 1 N HCl. The Mo and U fraction were collected separately, first with 2 mL 0.2 N HCl and then 2 mL of a 0.1 N HCl–0.3 N HF mixture, respectively. The Mo and U fractions were fluxed on a hotplate for 48 h in a 1 mL mixture of concentrated  $\text{HNO}_3$  and  $\text{H}_2\text{O}_2$ , to oxidize any residual organics, and then dried down. Finally, the purified Mo and U were re-dissolved in 0.3 N  $\text{HNO}_3$  and 0.2 N HCl, respectively, for mass spectrometry. Total procedural

blanks were  $\leq 100$  pg for both Mo and U so that corrections to isotope data for blank are negligible.

Mo and U isotope analyses were carried out at ETH Zürich, using a Neptune (Thermo-Finnigan) MC-ICP-MS equipped with an AridusII sample introduction system (CETAC) and a PFA nebulizer. Mass discrimination was corrected using the double-spike method as described previously for Mo (Siebert et al., 2003; Archer and Vance, 2008) and U (Andersen et al., 2016). All mass spectrometric errors were propagated through the double-spike calculation to obtain the final analytical uncertainty. Molybdenum isotope ratios are reported relative to SRM NIST 3134 =  $+0.25\%$  (Nägler et al., 2014) as follows:

$$\delta^{98}\text{Mo} = \left[ \frac{^{98/95}\text{Mo}_{\text{sample}}}{^{98/95}\text{Mo}_{\text{standard}}} - 1 \right] \times 1000 \quad (1)$$

The Mo double spike method was verified via the long-term analysis of an in-house Elemental Scientific ICPMS (CPI) standard with standard/spike ratios in the range 0.5–2, which has yielded a mean  $\delta^{98}\text{Mo}$  value of  $0.02 \pm 0.04\%$  (2SD) relative to SRM NIST 3134 =  $+0.25\%$  over the past 5 years ( $n = 117$ ).

The  $^{238}\text{U}/^{235}\text{U}$  and  $^{234}\text{U}/^{238}\text{U}$  data are presented in standard  $\delta$ -notation with the  $\%$  offset from (2) the bracketing CRM-145 standard and (3) secular equilibrium as follows:

$$\delta^{238}\text{U} = \left[ \frac{^{238/235}\text{U}_{\text{sample}}}{^{238/235}\text{U}_{\text{standard}}} - 1 \right] \times 1000 \quad (2)$$

$$\delta^{234}\text{U} = \left[ \frac{^{234/238}\text{U}_{\text{sample}}}{^{234/238}\text{U}_{\text{equilibrium}}} - 1 \right] \times 1000 \quad (3)$$

Verification of the U double spike method was achieved via repeated measurements of the in-house CZ–1 uraninite standard. The  $\delta^{238}\text{U}$  results for the CZ–1 standard during the period of analysis for this paper were  $-0.04 \pm 0.06\%$  (2SD,  $n = 24$ ) in agreement with previously reported values (Stirling et al., 2007; Andersen et al., 2015, 2016).

## 4. RESULTS

### 4.1. Namibian margin sediment geochemistry

The chemical and isotope compositions of sediments are summarized in Tables S2 and S3 and illustrated in Figs. 3, S1 and S2. The inner shelf and upper slope sediments have comparable TOC, with a range of 2.0–3.2 wt.% and 1.9–4.0



wt.%, respectively (Fig. 3). The sediments at the middle shelf site show the lowest TOC, with values ranging from 0.7 to 1.3 wt.%. All sediments show limited downcore variability in Mn/Al and Fe/Al ratios (Fig. S1). The Mn/Al ratios from all three stations are lower than the upper continental crust (UCC) (McLennan, 2001), implying reductive mobilization of Mn oxides from particulate material, either in the water column during transport downwards or within the sediment. From the inner shelf through the OMZ, Fe/Al ratios increase from values close to the UCC background for core 26010 (0.52–0.65) to values  $>2.0$  in cores 26030 and 26070. The relatively high  $Fe_{py}$  values for the

inner shelf and upper slope sediments may reflect Fe sulfide formation within the sediment as a result of  $H_2S_{aq}$  accumulation in the porewater (Fig. 3). In contrast, the highest Fe/Al ratios coincide with the lowest  $Fe_{py}$  in sediments at the middle shelf site, within the OMZ, indicating sedimentary Fe enrichment controlled by a phase other than sulfide.

#### 4.2. Authigenic molybdenum and uranium in the solid phase

The sediment depth profile of Mo/Al and U/Al ratios reveals moderate authigenic enrichment of Mo and U over the UCC background (Fig. S1). The  $\delta^{98}Mo_{bulk}$  range from

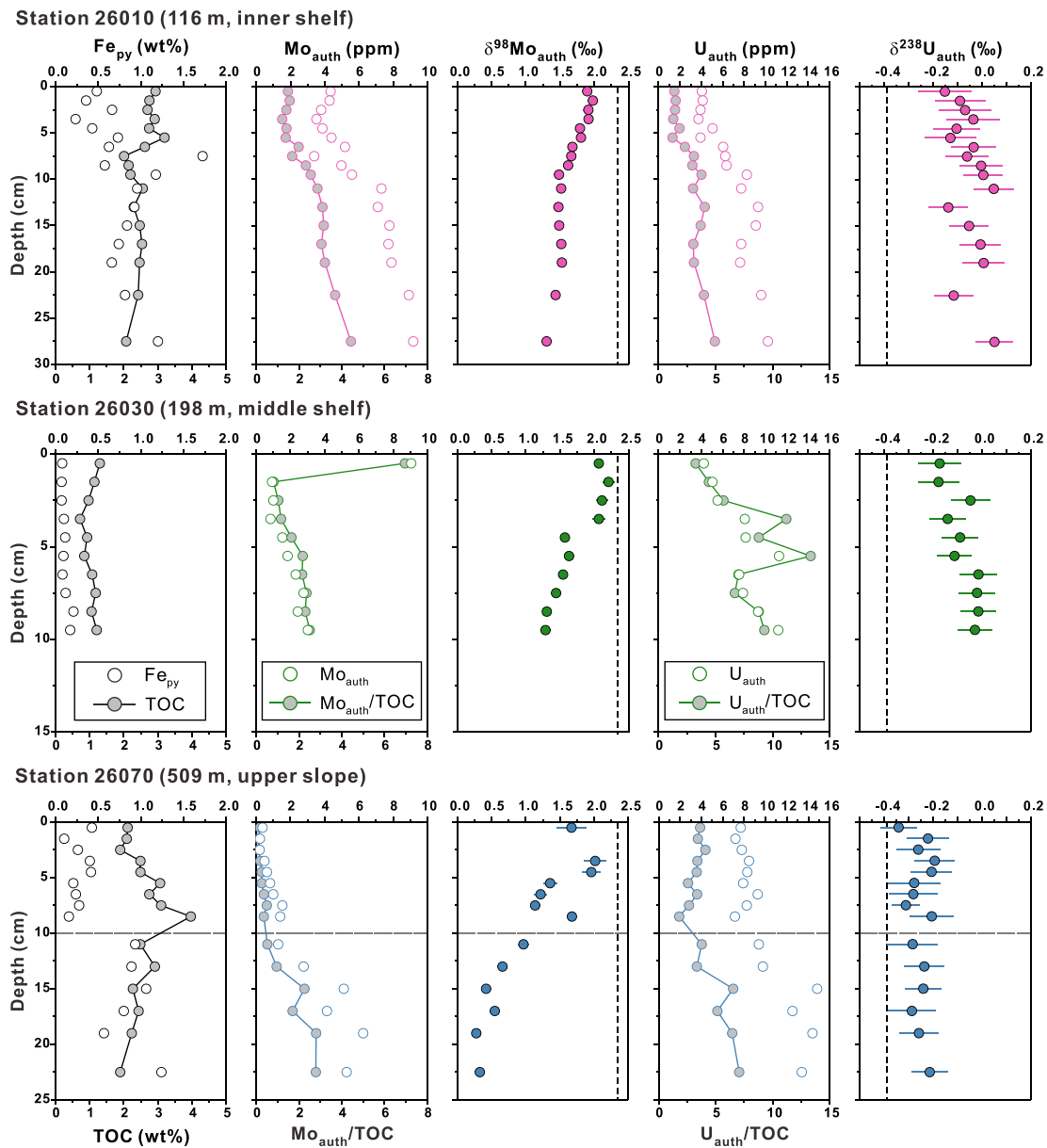


Fig. 3. Chemistry and isotope composition of the solid phase in Namibian margin sediments. The vertical dashed lines represent the average seawater isotope compositions ( $\delta^{98}Mo_{sw} = 2.34‰$ ;  $\delta^{238}U_{sw} = -0.39‰$ ). The sediment core from station 26070 is shown as divided into two chemical intervals by the horizontal dashed lines (10 cm depth) based on changes in TOC and  $Fe_{py}$  concentrations. All error bars on this and subsequent diagrams represent the 2SD reproducibility.

1.24‰ to 1.76‰ for station 26010, from 1.14‰ to 1.98‰ for station 26030, and from 0.28‰ to 1.34‰ for station 26070. In addition, all solid phase profiles show an overall decreasing trend in  $\delta^{98}\text{Mo}$  with depth. The  $\delta^{238}\text{U}_{\text{bulk}}$  range from  $-0.19\text{‰}$  to  $0.01\text{‰}$  for station 26010, from  $-0.20\text{‰}$  to  $-0.04\text{‰}$  for station 26030, and from  $-0.34\text{‰}$  to  $-0.21\text{‰}$  for station 26070, consistently higher than the seawater value of  $-0.39\text{‰}$ . The  $\delta^{238}\text{U}_{\text{bulk}}$  for each core show limited variation with depth, but display a general trend from low to higher values down core. The  $\delta^{234}\text{U}_{\text{bulk}}$  are much more variable for all cores (Table S3 and Fig. S2), ranging from 53‰ to 99‰ for station 26010, from 43‰ to 83‰ for station 26030, and from 24‰ to 85‰ for station 26070. These values are substantially below the seawater  $\delta^{234}\text{U}$  value of  $\sim 146\text{‰}$  (Andersen et al., 2010), suggesting an influence from detrital U in the bulk U concentration. Due to the uncertainty on the detrital bulk  $\delta^{234}\text{U}$ , which commonly has a  $\delta^{234}\text{U}$  below 0‰ (Andersen et al., 2016), it is not possible to use the bulk  $\delta^{234}\text{U}$  to calculate the fraction of detrital versus authigenic with confidence (Fig. S3).

To estimate the authigenic Mo and U concentration and the isotope composition of the authigenic Mo and U fractions ( $\delta^{98}\text{Mo}_{\text{auth}}$ ,  $\delta^{238}\text{U}_{\text{auth}}$ ), a correction for the detrital terrigenous siliciclastic and (for U only) biogenic carbonate fractions of the sediment is applied. For the authigenic Mo correction, a constant Mo/Al ratio of  $1.9 \times 10^{-5}$  (g/g) and  $\delta^{98}\text{Mo}_{\text{det}}$  of 0.3‰ of the detrital component are assumed (McLennan, 2001; Voegelin et al., 2014). The isotope ratio of the authigenic Mo can then be calculated as follows:

$$\delta^{98}\text{Mo}_{\text{auth}} = \frac{(\delta^{98}\text{Mo}_{\text{bulk}}[\text{Mo}]_{\text{bulk}} - \delta^{98}\text{Mo}_{\text{det}}[\text{Mo}]_{\text{det}})}{[\text{Mo}]_{\text{auth}}} \quad (4)$$

The authigenic U fraction is estimated by subtracting the detrital contribution using U/Al of  $3.5 \times 10^{-5}$  (g/g) (McLennan, 2001) and the biogenic carbonate contribution using a U/Ca ratio of  $3.25 \times 10^{-6}$  (g/g) (Andersen et al., 2014). The  $\delta^{238}\text{U}$  of the authigenic U fraction is then given by correcting the bulk  $\delta^{238}\text{U}$  for the detrital and carbonate fractions using a detrital  $\delta^{238}\text{U}_{\text{det}}$  of  $-0.3\text{‰}$  and a carbonate  $\delta^{238}\text{U}_{\text{carb}}$  of  $-0.4\text{‰}$  via the equation:

$$\delta^{238}\text{U}_{\text{auth}} = \frac{(\delta^{238}\text{U}_{\text{bulk}}[\text{U}]_{\text{bulk}} - \delta^{238}\text{U}_{\text{det}}[\text{U}]_{\text{det}} - \delta^{238}\text{U}_{\text{carb}}[\text{U}]_{\text{carb}})}{[\text{U}]_{\text{auth}}} \quad (5)$$

The uncertainties on the authigenic Mo and U isotope compositions were propagated by weighting the relative size of the detrital component following Andersen et al. (2014) (see Table S3 for details). The authigenic fraction dominates the sedimentary Mo budget for station 26010 (84–94%), but is variable for station 26030 (65–95%) and station 26070 (29–92%). The detrital U contribution to the sedimentary budget is found to be small for all cores, with more than 84% of the U being of authigenic origin for most sediments. The general dominance of the authigenic fraction for Mo and U generally results in small changes between the measured bulk and estimated authigenic  $\delta^{98}\text{Mo}$  and  $\delta^{238}\text{U}$  for sediments (Fig. S4). But the detrital correction has a particularly strong impact on  $\delta^{98}\text{Mo}_{\text{auth}}$  for samples

with low authigenic Mo fractions. Significant changes for  $\delta^{98}\text{Mo}_{\text{auth}}$  values are seen for the near-surface sediments at stations 26030 and 26070 with high detrital contribution (from 0.57‰ to 2.31‰ higher for  $\delta^{98}\text{Mo}_{\text{auth}}$ ), and a large uncertainty on authigenic  $\delta^{98}\text{Mo}$  (0.08–0.47‰ for 2SD). Two samples from station 26070 with  $\Delta^{98}\text{Mo}_{\text{auth-bulk}} > 1.0\text{‰}$  and large uncertainties are omitted from further discussion. For all samples, the sedimentary  $\delta^{238}\text{U}$  correction is relatively minor ( $<0.07\text{‰}$ ) and does not influence the following discussion.

### 4.3. Molybdenum and uranium in porewaters

The distributions of Mo and U concentration and isotope compositions in porewaters along 26°S are reported in Table S1 and shown in Figs. 4 and S2. The dissolved Mn, Fe, and  $\text{H}_2\text{S}$  for each core are also plotted, in order to constrain the diagenetic reactions in sediments (Fig. 4). All three cores are characterized by very low Mn concentrations, ranging between 17 nM and 123 nM. The porewater profiles of Fe show similar distribution patterns for stations 26010 and 26030, with the highest concentrations (up to 5  $\mu\text{M}$ ) near the sediment–water interface and a sharp drop to almost zero within the top few cm of the sediments. In these cores, dissolved  $\text{H}_2\text{S}$  reaches significant levels deeper in the core (Fig. 4). At station 26070, the dissolved Fe is more randomly distributed in porewaters and no dissolved  $\text{H}_2\text{S}$  was detected.

The dissolved Mo concentration and  $\delta^{98}\text{Mo}$  in porewater exhibit distinct down-core distribution patterns among stations. At station 26010, the porewaters display elevated dissolved Mo concentrations (141–326 nM) compared to seawater (110 nM) throughout a large portion of the core. The dissolved Mo is lower from a depth of about 15 cm, where the  $\text{H}_2\text{S}$  reaches high levels ( $>100 \mu\text{M}$ ). Porewater  $\delta^{98}\text{Mo}$  show a wide range (0.90‰ to 2.79‰) and the variation pattern mirrors that of Mo concentrations. At station 26030, the dissolved Mo concentrations are highly variable (123–875 nM) and show a pronounced peak at about 8 cm depth, while the porewater  $\delta^{98}\text{Mo}$  values fall into a relatively narrow range between 1.49‰ and 2.06‰. At station 26070, the Mo concentrations and  $\delta^{98}\text{Mo}$  values for the near-surface (0–9 cm) porewaters are relatively uniform at  $130 \pm 24$  nM and  $2.21 \pm 0.47\text{‰}$  (2SD;  $n = 9$ ). Below this depth, the Mo concentration increases linearly from 98 nM to 221 nM, while  $\delta^{98}\text{Mo}$  decreases from 2.57‰ to 1.11‰. Notably, the  $\delta^{98}\text{Mo}$  variation pattern closely mirrors Mo concentrations for all stations (Fig. 4).

The dissolved U concentration and  $\delta^{238}\text{U}$  in porewaters also exhibit distinct down-core distribution patterns among stations. At station 26010, both U concentration and  $\delta^{238}\text{U}$  have seawater-like values in the top 4 cm. The U concentration and  $\delta^{238}\text{U}$  are then elevated between 5 and 16 cm depth, with values ranging from 15.8 to 32.5 nM, and from  $-0.27\text{‰}$  to  $-0.04\text{‰}$ , respectively. Below 16 cm depth, the U concentration decreases downward from 27.4 to 6.3 nM, with  $\delta^{238}\text{U}$  shifting dramatically downwards from  $-0.27\text{‰}$  to  $-1.74\text{‰}$ . The porewaters from station 26030 display a wide range in U concentration, between 5.5 and 66.8 nM, with their  $\delta^{238}\text{U}$  varying from  $-0.51\text{‰}$  to  $0.26\text{‰}$ . The pore-

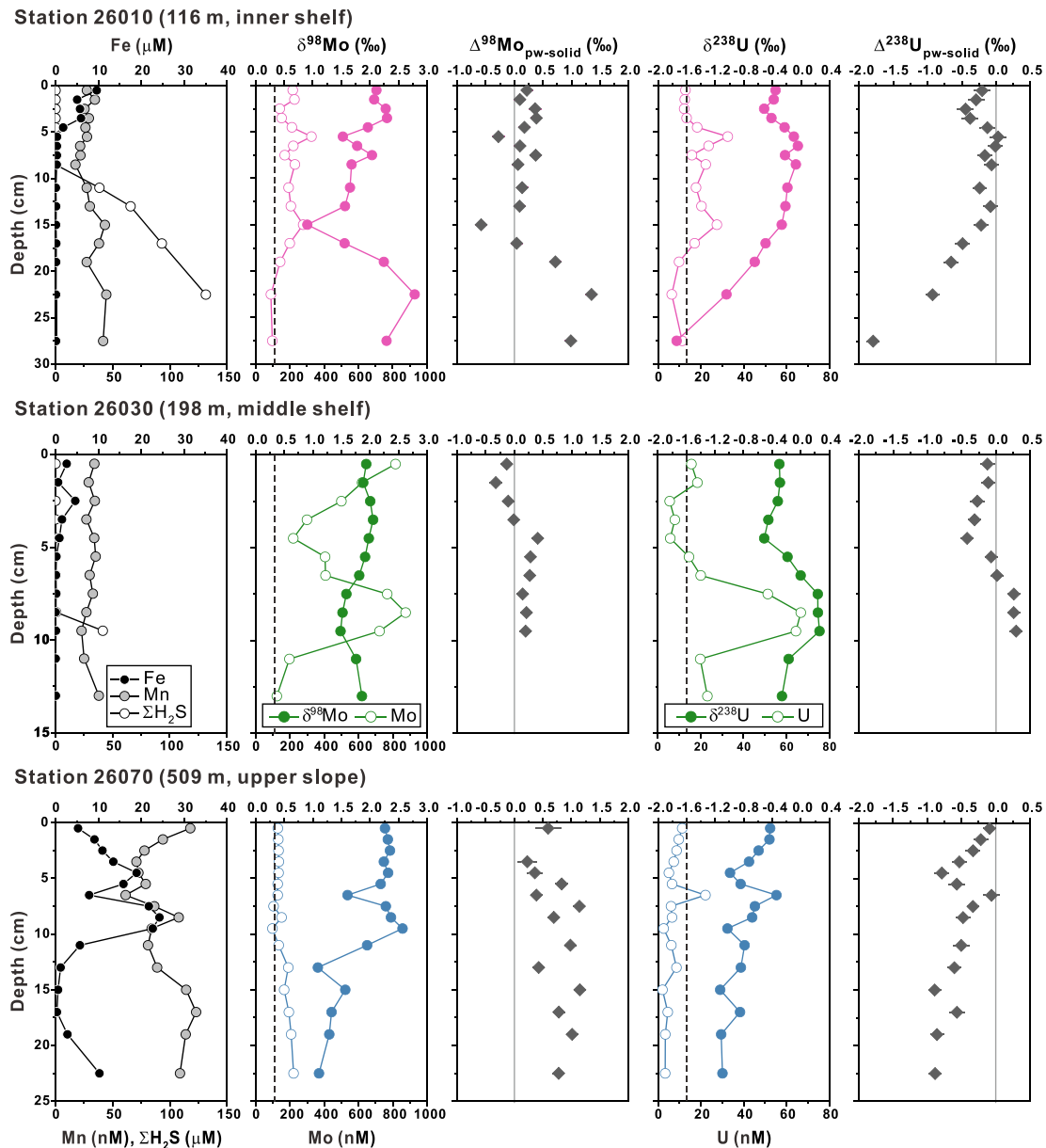


Fig. 4. Chemistry and isotope composition of porewaters in Namibian margin sediments. The vertical dashed lines represent the average seawater concentrations ( $[Mo]_{sw} = 110 \text{ nM}$ ;  $[U]_{sw} = 13.4 \text{ nM}$ ). The vertical solid lines indicate that  $\Delta^{98}Mo_{pw-solid}$  or  $\Delta^{238}U_{pw-solid}$  equals zero.

water U concentration profile does not show any regular U depletion with depth, and the general shape of the U concentration distribution is very similar to that observed for  $\delta^{238}U$ . Notably a maximum in U concentration (and maximum in  $\delta^{238}U$  values) is observed at a depth interval between 6 cm and 10 cm, co-incident with the peak in Mo concentrations. At station 26070, the U concentration of the porewaters range from 2.1 to 22.1 nM, and the  $\delta^{238}U$  range from  $-1.13\text{‰}$  to  $-0.34\text{‰}$ , displaying a generally decreasing trend with depth. It is noted that  $\delta^{234}U$  for all porewater samples fall within the range of modern seawater (Fig. S2), suggesting that most U is authigenic and that detrital contributions are minor.

The stations sampled for porewater concentrations only, in February 2019 (Table S4, Fig. 5), show similar features to the above. Manganese concentrations are also low except for the deepest station with the highest bottom water  $O_2$ , station 2 on the upper slope. Dissolved Mo and U concentrations, also here, are often well in excess of seawater throughout large portions of the cores, there are peaks beneath the sediment–water interface, and variations that are not correlated with either Mn or Fe. It is noteworthy that these similar and complex patterns are obtained from two different cruises and with completely different techniques – rhizon sampling versus slicing and centrifuging – to extract the porewaters.

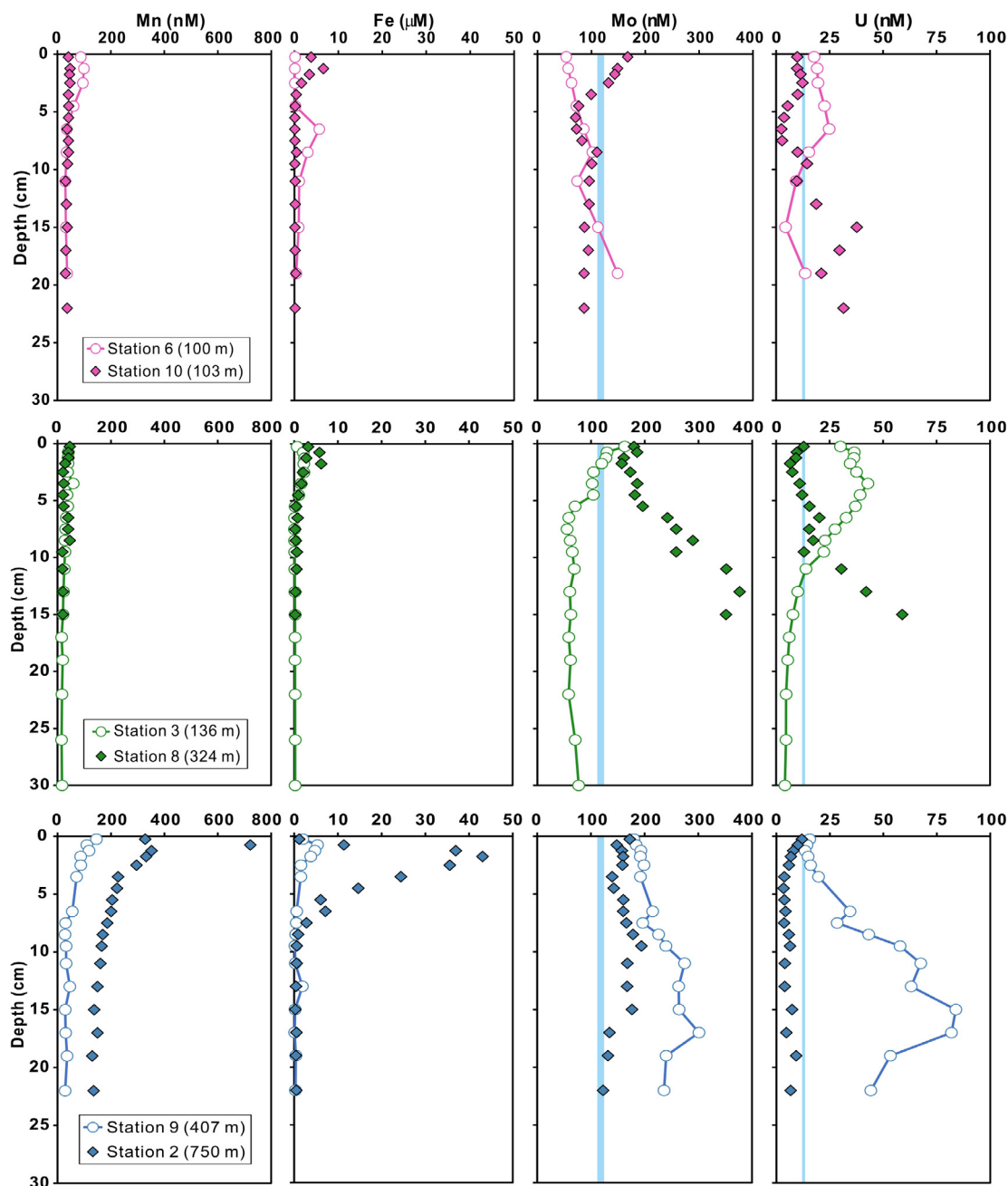


Fig. 5. Porewater profiles of Mn, Fe, Mo and U for stations 2, 3, 6, 8, 9, and 10. The vertical blue bands represent the range of bottom water concentrations for stations 2, 6, 8, 9, and 10 ( $[\text{Mo}]_{\text{BW}} = 113\text{--}124$  nM;  $[\text{U}]_{\text{BW}} = 12.6\text{--}13.3$  nM).

## 5. DISCUSSION

### 5.1. Sources of Mo and U to the Namibian margin sediment-porewater system

We have presented the first coupled Mo-U abundance and isotope dataset for both solid phases and porewaters in open-marine continental margin environments. Clearly, the solid phase of the sediment-porewater system is moderately enriched in Mo and U, as previously observed in this and other similar settings (e.g., [McManus et al., 2006](#);

[Poulson Brucker et al., 2009](#); [Scholz et al., 2011](#); [Abshire et al., 2020a, 2020b](#)); there has been addition of authigenic Mo and U to the solid phase. The ultimate source of these enrichments must be the aqueous phase, either the water column itself or porewaters. A striking feature of the porewater data is that Mo and U concentrations are also often enriched relative to seawater ([Figs. 4 and 5](#)). In the most general terms, the two broad processes that could lead to the transfer of Mo and U across the sediment-water interface and lead to the enrichment of the entire sediment-porewater system in Mo and U are: (1) transfer within

the aqueous phase from the water column to porewater, e.g., by diffusion (e.g., Anderson et al., 1989; Zheng et al., 2000; Scholz et al., 2011), followed by sequestration from the porewater into an authigenic particulate phase and; (2) transfer via a particulate phase that sequesters Mo and U from the water column itself (e.g., Shaw et al., 1990; Morford et al., 2007; Goldberg et al., 2012; Scholz et al., 2017, 2018; Eroglu et al., 2020; Hutchings et al., 2020), delivers it to the sediment-porewater system, and whose Mo and U inventory is partially remobilized into porewater. A third possibility that could explain the data for the particular sites studied here is represented by: (3) lateral transport of Mo- and U-enriched particulate material from elsewhere, given the spatial variability of the Namibian Margin system and the ubiquitous evidence for lateral sediment transfer (e.g., Inthorn et al., 2006a, 2006b).

As noted above, porewaters as sampled here are nearly always enriched in Mo and U relative to seawater. Thus, in the inner shelf core (26010) both Mo and U concentrations are significantly elevated in the upper 20 cm (Fig. 4). Site 26030 from the middle shelf exhibits Mo and U concentrations well in excess of seawater throughout the studied depth interval, and features a very pronounced peak at around 8 cm, with [Mo] up to 8x seawater. In core 26010, and around the 8 cm peak in core 26030, excess Mo and U concentrations are well correlated. Porewater Mo and U concentrations in core 26070 are lower, with [U] below seawater over most of the studied interval. But even here, [Mo] increases to double seawater concentrations over the depth interval 10–20 cm.

The fact that concentrations of Mo and U in porewaters are higher than seawater appears to rule out downward diffusional transport across the sediment–water interface, at least for the conditions at the time of sampling. It is theoretically possible that these conditions represent a snapshot in time only and, given the known temporal variability in the redox conditions on the Namibian margin (e.g., Borchers et al., 2005; Böning et al., 2020), that this snapshot is not representative of the longer term: that concentration gradients are periodically reversed to allow inward diffusion of Mo and U. We don't have any specific evidence for such a suggestion, and we note that other recent studies have reported porewater Mo concentrations in excess of 3000 nM at sites close to ours (Abshire et al., 2020b). Such an explanation encounters another difficulty: under the redox conditions at the sediment–water interface, as sampled here, there appears to be no obvious authigenic phase that would be stable and could act as a host for any Mo and U that might enter the sediment-porewater system following diffusion downwards from seawater, and yet the uppermost sediment is enriched in Mo and U.

We therefore suggest that mechanism (1) above unlikely explain the dataset presented here, even given the potential for significant temporal variability in the local redox conditions. Rather, we suggest, that a particulate source external to the sediment-porewater system must operate, via either mechanism (2) or (3) above. In the next section we explore the possible candidates for such a particulate source. Though none of these potential explanations work per-

fectly, temporal variability in redox leading to sequestration by bottom water sulfide is the most viable.

## 5.2. Potential particulate Mo and U sources to the Namibian margin sediment-porewater system

### 5.2.1. The lack of an Fe-Mn (oxyhydr)oxide shuttle

One obvious candidate for a particulate source of Mo is Mn oxides, which scavenge Mo from the upper oxic portion of the water column and potentially deliver it to the sediment, where such oxides reductively dissolve and release Mo to porewater (e.g., Algeo and Tribouillard, 2009). However, there are several reasons why we argue such a process cannot explain our data. First, Mn concentrations are extremely low in these Namibian porewaters (Figs. 4 and 5), with the exception of one site on the slope (Station 2, Fig. 5). Where Mn oxide is clearly implicated as a source of Mo, porewater Mn is high and ratios of excess Mo (over seawater) to Mn are around 0.001–0.01 mol/mol (e.g., Goldberg et al., 2012; Eroglu et al., 2020), consistent with measured ratios for solid phase Mn oxides (Manheim and Lane-Bostwick, 1991). In the porewaters studied here (Fig. 4), ratios of excess Mo to Mn are orders of magnitude higher, at 1–8 mol/mol than expected from a Mn oxide source. The lack of significant delivery of Mn oxide associated Mo to the sediment–water interface is supported by low sedimentary Mn/Al for all three sites (Fig. S1). Thus, in congruence with conclusions from other upwelling margins that feature an intense water column OMZ (e.g., Böning et al., 2004; Scholz et al., 2011), it appears that particulate Mn oxides are reductively dissolved during sinking through the OMZ, and that they never reach the sediment–water interface.

Scholz et al. (2017) note very high authigenic Mo concentrations (up to 50 ppm) in sediment cores collected at 100–700 m on the Peruvian margin, associated with a rather narrow range of  $\delta^{98}\text{Mo}$ , between 1.25‰ and 1.52‰. These authors suggest that Mo is delivered to the sediment surface by Fe (oxyhydr)oxides, most of which precipitate in the nitrogenous water column due to oxidation of sediment-derived dissolved Fe with nitrate as a terminal electron acceptor. In this mechanism, a fraction of the Fe and Mo is cyclically re-dissolved, and eventually re-precipitated through interaction with porewater sulfide. Some aspects of the sediment data obtained here for Namibian margin cores are consistent with this explanation of sedimentary Mo enrichment. For example, there is strong sedimentary Fe enrichment at sites 26030 and 26070, though not at site 26010 (Fig. S1). Authigenic Mo in the solid phase of the Namibian sediment and in porewater is mostly isotopically lighter than seawater, as expected from Fe-oxide-associated Mo (Goldberg et al., 2009).

But there are aspects of the co-variation of Fe and Mo in the porewater that argue against an impact of an Fe-oxide-associated mechanism, a lack of co-variation that cannot be explained by decoupling of Mo and Fe concentrations due to the reactivity of Fe with dissolved sulfide. For example, iron concentrations are as high as 10  $\mu\text{M}$  in the porewater over the upper 5 cm of core 26010, whereas the Mo enrich-

ment in excess of seawater extends well beneath this to 20 cm. Low aqueous Fe over part of this interval (beneath 10 cm) can be attributed to precipitation as sulfide, but over other parts Fe and H<sub>2</sub>S concentrations are both below the detection limit. The upper peak in porewater Mo concentration in core 26030 is associated with detectable porewater Fe concentrations, but the peak centered on 8 cm is not. Again, this decoupling of Mo and Fe cannot be attributed to removal of Fe to a sulfide while Mo remains in solution, because neither Fe nor H<sub>2</sub>S are detected at the Mo peak (Fig. 4). In core 26070, porewater Mo concentrations are not elevated over the upper 12 cm of the core where the Fe peak occurs. Instead, they begin to increase at or below 15 cm where porewater Fe concentrations are low, again in the absence of detectable H<sub>2</sub>S. Thus, porewater Fe and Mo concentrations are decoupled in the Namibian porewater profiles, in ways that cannot be explained by co-precipitation of Fe with dissolved sulfide, and argue against an Fe (oxyhydr)oxide source for Mo.

It is also noted that both excess U in porewater and solid phase U are isotopically heavier than seawater, in the opposite direction to that expected from Fe-Mn (oxyhydr)oxide sources (e.g., Stirling et al., 2007; Weyer et al., 2008; Wang et al., 2016). Overall, these arguments rule out an Fe-Mn (oxyhydr)oxide shuttle as a dominating particulate source of Mo and U to the Namibian sediment-porewater system.

### 5.2.2. The potential impact of intermittently sulfidic conditions

As noted in Section 2, an intriguing aspect of the Namibian upwelling margin is the temporal variability in productivity, with periods of high productivity leading to significant H<sub>2</sub>S in bottom water. Borchers et al. (2005) previously hypothesized that this could trigger the precipitation of a variety of trace elements within the water column. Through this mechanism, dissolved molybdate could be converted to thiomolybdate, permitting its scavenging by organic matter (e.g., Algeo and Lyons, 2006; Dahl et al., 2017) or triggering co-precipitation with Fe and S in a mixed Mo-Fe-S phase (Helz et al., 2011). Although elevated water column H<sub>2</sub>S, by itself, does not lead to U reduction (e.g., in the Black Sea; Anderson et al. 1989), the resuspension of sediment and/or organic matter that occurs during some of these bottom water sulfidic events would provide particulate surface area to catalyze the U reduction process (Anderson et al., 1989). Remobilization of this authigenic pool of Mo and U could then create the observed enrichments in the porewaters. We note that free porewater sulfide right at the sediment-water interface might also lead to sequestration of Mo and U to particulates, without necessarily invoking pervasive sulfide in bottom water itself. This is, however, a quantitative rather than a qualitative difference: both scenarios require significant changes in redox conditions.

Whether such a mechanism could operate for the cores we have studied is currently unclear, in part because of the lack of a full characterization of the spatial and temporal variability of the BUS (Nelson and Hutchings, 1983). Catastrophic sulfide eruptions are best known from the diatomaceous mud belt further north, at 19–25°S. Here,

porewater H<sub>2</sub>S concentrations are at >10 mM levels at depths  $\geq 1$  m beneath the sediment-water interface (e.g., Emeis et al., 2004), much higher than the maximum 0.15 mM levels we observe in the upper 20 cm here. Brüchert et al. (2006) favor diffusive transport of H<sub>2</sub>S from the sediment at latitudes south of 24°S. On the other hand, where porewater H<sub>2</sub>S has been sampled deep in cores close to those studied here, at 26°S, it is also at 10 mM levels (e.g., Fossing et al., 2000). Whatever the exact process, remote sensing approaches (e.g., Weeks et al., 2002, 2004; Ohde et al., 2007) have repeatedly detected water column H<sub>2</sub>S in the coastal region at 26°S.

The substantial solid phase sulfide and high TOC observed in core 26010 (Fig. 3) are consistent with past sulfidic eruptions. Moreover, low Fe/Al ratios in this core (Fig. S1) would potentially prevent sequestration of H<sub>2</sub>S, produced during short periods involving high rates of bacterial sulfate reduction, from being oxidized and trapped by reactive iron (Brüchert et al., 2003, 2006; Borchers et al., 2005). Though dissolved sulfide is generally not detected at all in the porewaters at site 26030 on the middle shelf (Fig. 4), this core also exhibits non-zero amounts of solid sulfide (Fig. 3). This site also has the most complex porewater patterns of the three studied here, with the porewater peak in Mo and U concentrations at 8–9 cm, at levels that are a factor of 5–8 higher than seawater, demanding a source within the sediment. It may also be significant that the one depth where sulfide is detected is at 10 cm, just below the Mo-U peak, and perhaps indicating a common source of Mo, U and reduced sulfide from a solid phase that is breaking down.

For both sites 26030 and 26070, sedimentary Fe/Al ratios are high and correlated with enrichments in potassium (Fig. S5), consistent with previous studies highlighting the formation of authigenic glauconite (Böning et al., 2020). Glauconite formation requires high dissolved Fe, both Fe<sup>2+</sup> and Fe<sup>3+</sup>, in porewater at reduced sedimentation rates (Scholz et al., 2014), also suggesting the redox potential of the middle shelf and upper slope sites at 26°S may not, even periodically, be appropriate for H<sub>2</sub>S buildup. We also cannot rule out, however, the possibility that Mo and U are supplied to the sediment-porewater system at these sites via lateral transport of particulate matter from elsewhere, in sulfide or another phase, a possibility we assess in the next section.

### 5.2.3. The potential influence of cross-shelf lateral transport and redeposition

A final possibility for explaining the enrichment of the sediment-porewater system in Mo and U at the sites studied here lies in the spatial variability in the Namibian Margin system. A number of studies have demonstrated that extensive lateral transport of particles in nepheloid layers, from the shelf to deeper waters, occurs along the Namibian margin (e.g., Inthorn et al., 2006a, 2006b). A recent study by Abshire et al. (2020a) examined the erosion, lateral transport, and redeposition of sediments across a shelf-to-slope transect at ~25.5°S. These authors found that sedimentary U and TOC were coupled on the shelf, that erosion out-competed authigenic U uptake at the shelf break, and a

pronounced decoupling of U and TOC for the slope sediments. Accordingly, it may be inappropriate to attempt to explain many features of the current dataset on the shelf break and slope through processes occurring *in-situ*, given that the area of final burial may be displaced from that with the vertical particle supply.

In comparison to the areas with a prominent depocenter further north (e.g., [Inthorn et al., 2006a, 2006b](#)), the potential for shelf-to-slope lateral particle transport is less clear at 26°S. An important characteristic of laterally-transported sediment is anomalously high TOC ([Inthorn et al., 2006b](#)) coupled to anomalously low U/TOC ratios due to oxidative loss of U during transport ([Abshire et al. 2020a](#)). [Fig. 6](#) examines the relationships between Mo-U systematics and TOC for all the cores studied. Molybdenum is clearly least enriched in near-surface sediments on the slope regardless of high TOC ([Fig. 6a](#)). But this observation cannot be definitively ascribed to Mo loss during lateral transport. Indeed, if Mo was being released back into the water column through oxidation, the oxidation of the reduced U phases should also occur, which is not supported by our U data ([Fig. 6b](#)). Instead, higher enrichment of U relative to Mo in core 26070 is more likely attributed to the *in-situ* suboxic conditions at this site, consistent with the general notion that onset of authigenic U enrichment

occurs under less intensely reducing conditions than that of Mo ([Algeo and Tribouillard, 2009](#)).

Additional evidence for the local redox rather than lateral transport controls on sedimentary Mo and U enrichments comes from the respective isotope systems. For the entire  $\delta^{98}\text{Mo}_{\text{auth}}$  dataset measured in this study, except for one outlier, significant correlations are observed between  $\delta^{98}\text{Mo}_{\text{auth}}$  and  $\text{TOC}/\text{Mo}_{\text{auth}}$  for each core ([Fig. 6c](#)), following the expected trend for early diagenetic enrichments of Mo (e.g., [Scholz et al., 2017](#)) in that the ongoing incorporation of Mo into sediment results in isotopically lighter Mo. The systematics on the same diagram for U are not clear ([Fig. 6d](#)), partly due to the smaller dynamic range in U isotope compositions relative to analytical uncertainty. Importantly, the diagrams also show that both Mo and U isotope data for slope sediments apparently plot outside of the fields typical for the shelf sediments ([Fig. 6c and d](#)). This result contrasts with the recent suggestion that the isotope signature in redeposited slope sediments should reflect its primary shelf depositional redox conditions, at least for U ([Abshire et al., 2020a](#)).

The shelf sediments in [Abshire et al. \(2020a\)](#) show systematics in  $\delta^{238}\text{U}$  and U concentration vs. depth that are consistent with U uptake and isotope fractionation via U diffusion across the seawater-sediment interface and

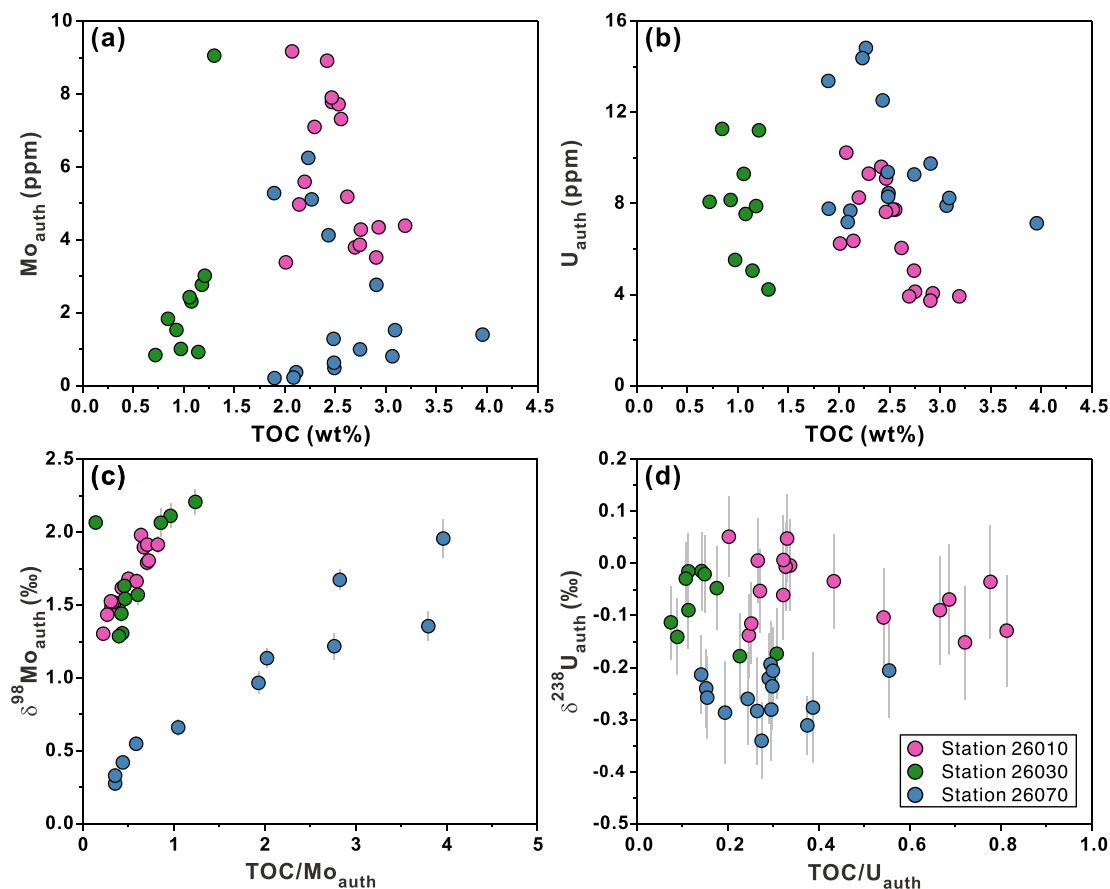


Fig. 6. Cross-plots of (a)  $\text{Mo}_{\text{auth}}$  versus TOC, (b)  $\text{U}_{\text{auth}}$  versus TOC, (c)  $\delta^{98}\text{Mo}_{\text{auth}}$  versus  $\text{TOC}/\text{Mo}_{\text{auth}}$  and (d)  $\delta^{238}\text{U}_{\text{auth}}$  versus  $\text{TOC}/\text{U}_{\text{auth}}$  for Namibian margin sediments.

increasing U uptake at depth. Such a systematic process requires a steady-state U uptake which, for this site, may be linked to the strong OMZ development above the core site. In contrast both the slope sediment core in the [Abshire et al. \(2020a\)](#) and the three sediment cores in this study are situated in more dynamic redox settings, which would not necessarily lead to clear correlations with  $\delta^{238}\text{U}$  and U vs. TOC, possibly the contrary. These findings suggest that, from an isotope perspective, Mo and U systematics primarily respond to the local redox conditions at each site, despite the potential influence of lateral transport and redeposition.

### 5.3. Response of Mo and U isotope systematics to early diagenesis under dynamic redox conditions

Diffusive delivery has been widely invoked as a driver for enrichment in authigenic Mo and U in reducing settings (e.g., [Anderson et al., 1989](#); [Zheng et al., 2000](#); [Scholz et al., 2011](#)). Such a process can only explain the complex patterns of porewater variability in Mo and U concentrations observed here via temporal variability, leading to periodic reversal of porewater gradients versus those observed here and in other studies (e.g., [Abshire et al., 2020b](#)). An alternative process, also invoking temporal variability, is represented by Mo and U delivery to sediment in a particulate phase that is then partially remobilized. As discussed in the previous section, both local bottom water sulfidic events or lateral transport could provide those particles but both these explanations require further investigation. Given the dynamic and complicated spatial and temporal redox conditions across the Namibian shelf and other OMZs, it is difficult to rule out the significance of a range of processes (diffusion, lateral redistribution, sulfidic events) for authigenic Mo and U enrichments at different locations.

The observations presented for these Namibian shelf cores strongly emphasize the impact of early diagenesis under dynamic redox conditions on sedimentary Mo and U cycling and associated Mo-U isotope systematics. Overall, the specific scenario favored here involves: (a) a predominantly steady-state diffusive redox situation unlike the current setting we observed here but interrupted by; (b) transient more reducing conditions that result in horizons within the sediment that are enriched in authigenic Mo and U by particulate supply; (c) the oxidative remobilization of these authigenic reservoirs to provide local dissolved sources to porewater and; (d) diffusive transfer through porewaters away from these local sources. It is important that, in this scenario, a solid reservoir controls and buffers the porewater most of the time. We note that mass balance is also in favor of this suggestion: for example, for the 8 cm Mo and U peak in porewater concentrations in core 26030, the concentration of Mo in the solid phase is more than 30 times that in the aqueous phase ([Tables S1 and S2](#)). This also has the consequence that the interpretation of the large and short length scale changes in the abundance of Mo and U in porewaters do not require significant correlative variation in the size of the solid authigenic phase from which they derive – e.g. organic material.

The additional key process, that finally sets the systematics in the sediment, is uptake into a new authigenic phase at depth within the core and at the end of the diffusion pathways mentioned above. The simplest manifestations of this set of processes are for U at sites 26010 and 26070. At site 26070, with the exception of one spike at 6–7 cm, porewater U concentrations generally decrease, and  $\delta^{238}\text{U}$  decreases, downwards ([Fig. 4](#)). This profile is closest to control by a single process: diffusion downwards and uptake into an authigenic phase at depth, perhaps beneath the sampled depth interval, with an isotope fractionation.

At site 26010, porewater U concentrations are elevated in the upper 20 cm of the profile. Where concentrations peak significantly above seawater, the difference between the porewater and the solid is very close to zero ( $\Delta^{238}\text{U}_{\text{pw-solid}}$ , [Fig. 4](#)), consistent with control of porewaters by particle dissolution. Beneath about 20 cm, U concentrations decrease below the seawater value and  $\delta^{238}\text{U}_{\text{pw}}$  decreases, again consistent with diffusive transfer of U from the source close to the top of the sediment along a concentration gradient to a sink into a second authigenic phase at depth. Given high porewater  $\text{H}_2\text{S}$  concentrations and significant pyrite contents deeper in this core, this second authigenic phase is likely to be a sulfide or, for U, to be associated with microbially-produced Fe(III) and sulfate reductants ([Lovley et al., 1991](#); [Zheng et al., 2002](#)). The U data for site 26030 are more complex, including a very sharp and pronounced porewater peak at about 8 cm with U concentrations 4–5 times in excess of seawater ([Fig. 4](#)). Away from this peak, concentrations and isotope compositions change rapidly both upwards (we suggest back to seawater values) and downwards, possibly again reflecting uptake associated with Fe(III) and sulfate reduction given the first detectable porewater  $\text{H}_2\text{S}$  just below the porewater concentration peak.

The impact of the two main competing processes on U and its isotopes are further examined in  $\ln(U)$  versus  $\delta^{238}\text{U}$  space in [Fig. 7a](#). Though there is scatter, and though there is one anomalous analysis, a lot of the U data lie close to a Rayleigh fractionation trend that we suggest represents uptake into a secondary authigenic phase at depth – related to microbial Fe(III) and sulfate reduction – that prefers the heavy isotope by about 0.6‰, in good agreement with diffusion-limited porewater U reduction in other anoxic sediments (e.g., [Andersen et al., 2014, 2017](#)). The remainder of the U data involve higher concentrations than seawater and heavier isotopes, which we suggest represents mixing between seawater and U derived from the oxidative breakdown of a reduced U phase. Of course, the superimposition of these two processes means that none of the data fit either of these two processes perfectly, leading to the moderate scatter seen in [Fig. 7a](#).

In contrast to uranium, the Mo dataset is dominated by porewater concentrations higher than seawater ([Fig. 7b](#)), so that the source of Mo to porewater from the phase formed during more reducing conditions must be much more important than for U, perhaps due to a Mo/U ratio that is substantially higher than seawater. The greater importance of this source control, the variability in the exact loca-



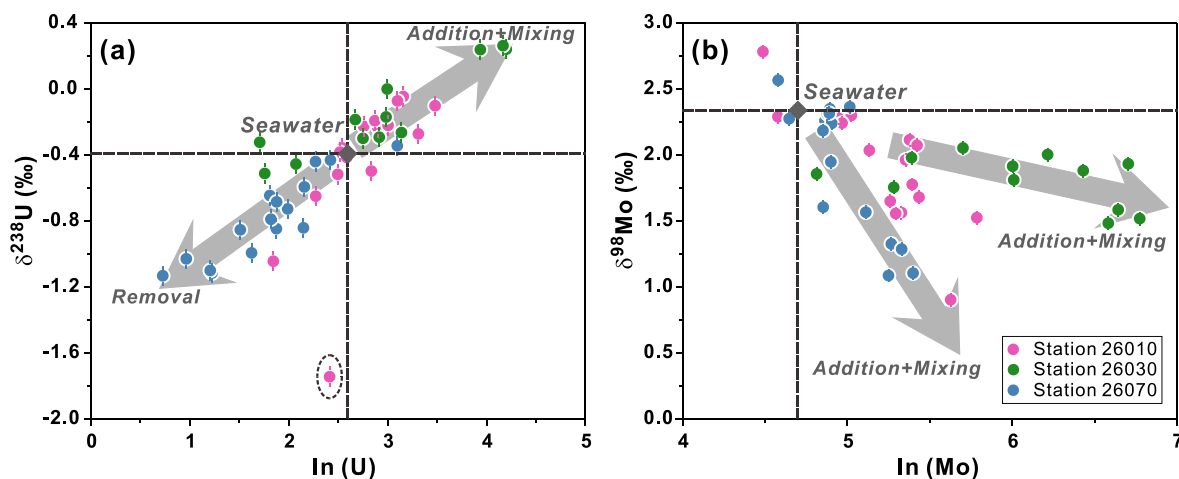


Fig. 7. Cross-plots of (a)  $\delta^{238}\text{U}$  versus  $\ln(\text{U})$  and (b)  $\delta^{98}\text{Mo}$  versus  $\ln(\text{Mo})$  for porewaters. The grey arrows represent the two main processes suggested here to lead to redistribution of Mo and U, and their isotopes, within the sediment-porewater system. A point highlighted by black dashed circle in panel (a) represents the deepest porewater sample from station 26010 with  $\delta^{238}\text{U}$  and  $[\text{U}]$  that are offset from the Rayleigh fractionation trend during U removal.

tion of sources within each core, and the fact that this variable source interferes to a much greater degree with diffusion away from peaks to zones of uptake, leads to greater scatter for the Mo data than for U. In particular, for example, the core with the pronounced porewater Mo peaks (26030) exhibits the impact of mixing away from a simple single-process scenario involving preferential uptake of the light isotope into a sulfide phase at depth. The fact that the authigenic Mo at depth is isotopically light is consistent with the non-quantitative conversion to thiomolybdate in the sulfidic portion of the cores (e.g., Tossell, 2005; Kerl et al., 2017; Matthews et al., 2017).

In summary, the data presented here for the Namibian margin in conjunction with previous studies (e.g., Zheng et al., 2000, 2002; Scholz et al. 2011, 2017, 2018) highlight the importance of temporally and spatially dynamic redox conditions in governing early diagenesis of Mo and U in sediments. Mo and U appear to initially be delivered and enriched in sediments during periods of high-productivity and reducing conditions. The Mo and U are then redistributed within the sediment via oxidative dissolution of reduced phases, followed by diffusion along concentration gradients. Diffusion is generally downwards towards a sulfidic sink, but multiple porewater peaks within the sediment can lead to concentration gradients and diffusion both upwards and downwards.

#### 5.4. Implications for coupling Mo-U isotopes as a paleoredox proxy

It has been demonstrated that coupled Mo and U isotopes hold advantages over a single isotope system for understanding depositional and redox conditions in the modern and ancient oceans (Asael et al., 2013; Kendall et al., 2015, 2020; Bura-Nakić et al. 2018; Lu et al., 2020; Stockey et al., 2020). In Fig. 8, the dataset for the Namibian margin is compared to data for modern euxinic basins in this coupled Mo-U context. The inner shelf sediments in

our dataset are characterized by moderate Mo and U enrichments at a Mo/U ratio close to that of seawater (Fig. 8a). In contrast, the data for both the middle shelf and slope sediments start at a very low Mo/U ratio, indicative of preferential uptake of U over Mo under largely sub-oxic conditions, but define a steep trend as representing decreasing benthic redox potential (Algeo and Tribovillard, 2009). Notably, none of the data plot along a trend for the ‘Fe-Mn particulate shuttle’ that has been observed in Peru margin sediments (e.g., Scholz et al., 2011), providing additional evidence that the light Mo isotope values in these Namibian margin sediments are not the result of the operation of an Fe-Mn particulate shuttle. The most significant feature of our isotopic dataset is the pronounced inverse correlations between the Mo and U isotope data, with two separate trends towards lower  $\delta^{98}\text{Mo}$  and higher  $\delta^{238}\text{U}$  (Fig. 8b). Such inverse correlations have been observed in modern semi-restricted euxinic basins, and ancient data are often interpreted in the context of this kind of setting. It is thus very significant that, qualitatively, the same feature is observed for the first time in open-marine continental margin sediments.

According to one framework for restricted basins, inverse  $\delta^{98}\text{Mo}$  and  $\delta^{238}\text{U}$  trends are dominantly the result of variation in water column  $\text{H}_2\text{S}$  and bottom water renewal time (e.g., Andersen et al. 2018; Bura-Nakić et al., 2018; Brüske et al. 2020). In settings with relatively high  $\text{H}_2\text{S}_{\text{aq}}$  and slow bottom water renewal rates, authigenic Mo and U typically show Mo/U ratios and isotope compositions close to the open ocean, due to near quantitative U and Mo uptake (e.g., Kyllaren Fjord; Lake Rogoznica). In contrast, in settings with relatively low  $\text{H}_2\text{S}_{\text{aq}}$  and fast bottom water renewal rates, the expressed isotope fractionations are greater due to non-quantitative removal, (with isotopically light Mo and U that is up to  $\sim 0.6\text{‰}$  heavier) and authigenic Mo/U ratios are higher (e.g., Cariaco Basin and Saanich Inlet). More recently, Brüske et al. (2020) have demonstrated that variations in the local depo-

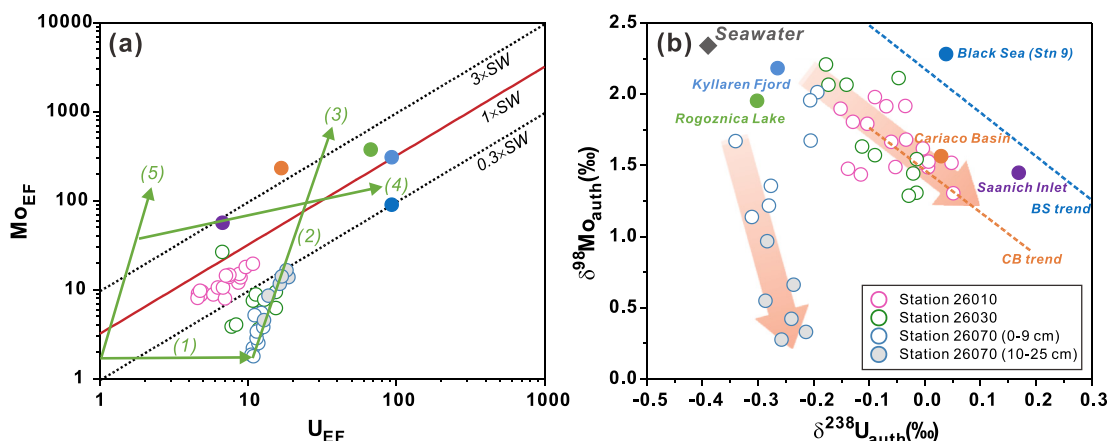


Fig. 8. Cross-plots of (a) Mo and U enrichment factors (EF) and (b) authigenic Mo and U isotope compositions for Namibian margin sediments compared to euxinic basins (from Bura-Nakić et al., 2018 and references therein; Brüske et al., 2020). (a) The solid red line depicts the relative proportion of Mo and U in seawater (weight ratio of  $[Mo]_{sw}/[U]_{sw} = 3.2$ ), with deviations from the seawater ratio shown as dashed black lines. The light green arrows show schematic evolution in enrichment factor trajectories based on physical and chemical controls on water masses (Algeo and Tribovillard, 2009), which are marked as (1) ‘Suboxic’, (2) ‘Redox variation’, (3) ‘Sulfidic, open marine’, (4) ‘Strongly restricted basin’, and (5) ‘Particulate shuttle’. (b) The arrows depict the anti-correlation between authigenic Mo and U isotope data for Namibian margin sediments, including shifts from seawater value (filled grey diamond) to higher  $\delta^{238}U$  and lower  $\delta^{98}Mo$  values. The blue and orange dashed lines depict the best-fit correlations between  $\delta^{98}Mo$  and  $\delta^{238}U$  for Black Sea sediment samples deeper than 3 cm and Cariaco Basin sediment samples deeper than 10 cm (Brüske et al., 2020), respectively.

sitional environment of Black Sea and Cariaco Basin can drive inverse correlations between  $\delta^{98}Mo$  and  $\delta^{238}U$  in sediments, but following different trends (Fig. 8b). The variation may be due to a range of smaller effects on the U isotope compositions, including minor U reduction and isotope fractionation in the water column (Brüske et al., 2020), variable U isotope fractionation in anoxic sediments due to differences in organic-carbon deposition and sedimentation rates (Lau et al., 2020), and addition of isotopically-light U associated with organic matter deposition (Abshire et al. 2020a).

The Namibian margin is very different from the above systems in terms of its geometry and redox structure, yet Mo-U isotopes show the same inverse correlations. Our interpretation of Mo and U isotope fractionation in these Namibian margin sediments, guided by the porewater data, is that redox-driven diffusion across the seawater-sediment transition may not be the dominant process. Instead, the key process dictating the initial Mo-U enrichment and isotopic composition is the occurrence of transiently more reducing conditions (i.e., enhanced productivity and sporadic bottom water  $H_2S$ ), followed by remobilization to porewater, diffusion and re-precipitation with an associated isotope fractionation. The general decrease of  $\delta^{98}Mo$  and increase in  $\delta^{238}U$ , coupled with greater Mo and U enrichment with sediment depth, is caused by intermittently high porewater  $H_2S$ , U and Mo mobility by diffusion, and formation of reducing (U) and sulfidic (Mo) authigenic phases deeper in the sediments. Hence, the conditions at the Namibian margin produce similar data patterns as for restricted or semi-restricted euxinic basins, but via a different set of processes.

This inferred mechanism could lead to a range of specific trends in individual marine settings, where both Mo-U con-

centration and inversely correlated  $\delta^{98}Mo$ - $\delta^{238}U$  depend specifically on: 1) the amount and isotope composition of the initial particulate authigenic U and Mo and; 2) the redox potential and  $H_2S_{aq}$  levels of the local porewater environment. In this context, the steeper trend toward lower  $\delta^{98}Mo$  seen for the Namibian slope sediments, as highlighted in Fig. 8b, arises because of the occasional occurrence of mildly sulfidic conditions upon OMZ fluctuations, which leads to isotope fractionation associated with the incomplete conversion of molybdate to thiomolybdate species. It seems that the negative trends from slope environments would be more similar to shelf settings if an OMZ is larger and more stable (Fig. 8b). Thus, negative  $\delta^{98}Mo$ - $\delta^{238}U$  trends like those in Fig. 8b could be of great use for the reconstruction of OMZ variability and redox oscillations in ancient open marine settings.

The sporadic bottom water  $H_2S$  would occur in a more open-system particle-rich environment compared to sediment porewaters, which could lead to reduced authigenic U with high  $\delta^{238}U$  (i.e.,  $\Delta^{238}U$  of  $\sim +1.2\%$  rather than the diffusion limited value of  $\sim +0.6\%$ ). Similarly, the authigenic Mo could have a  $\delta^{98}Mo$  that covers a range of compositions extending well below seawater, dependent on the exact  $H_2S_{aq}$  levels. Thus, a range of authigenic  $\delta^{238}U$  and  $\delta^{98}Mo$  could be expected, but with a larger range of isotope compositions than observed in modern restricted euxinic basins. A range of paleo-studies have recently documented an inverse correlation between Mo and U isotope compositions in organic-rich sediments, similar to those observed in the modern euxinic basins, but extending to higher  $\delta^{238}U$  and lower  $\delta^{98}Mo$  (Andersen et al. 2020; Cheng et al. 2020; Kendall et al. 2020). These authors suggest possibilities for the higher  $\delta^{238}U$ , in terms of water column U reduction (Kendall et al. 2020) or U reduction via high pro-

ductivity and formation of an organic floccule layer (Andersen et al. 2020; Cheng et al. 2020). However, in light of our new data, extreme (high)  $\delta^{238}\text{U}$  and (low)  $\delta^{98}\text{Mo}$  could reflect dynamic open-marine environment settings where sporadic bottom water  $\text{H}_2\text{S}$  may provide the right conditions for particulate uptake of both Mo and U, with the Mo and U isotope composition ultimately dictated by how quantitative the uptake process is for the two elements. Therefore, detailed paleo-geographical and geochemical information need to be combined to understand and interpret Mo-U isotope systematics from ancient sediments.

## 6. CONCLUSIONS

In this paper we have presented new Mo and U concentration and isotope data for both solid phases and porewaters in sediments from three sites along a transect across the

Namibian margin. Our findings are summarized in a conceptual model that invokes temporal variability in local redox conditions (Fig. 9a; i.e., enhanced productivity and sporadic bottom water  $\text{H}_2\text{S}$ ) and relatively less reducing periods (Fig. 9b; i.e., suboxic conditions). Particulate Mo and U scavenging by Fe-Mn oxides in the water column is ruled out as a major mechanism for Mo and U delivery to these sediments. Lateral particle transport and redeposition, previously recognized on the Namibian margin, also appear not to significantly affect the Mo-U systematics of these sediments. Instead, Mo and U abundances and isotope compositions require temporally dynamic redox conditions, with these elements most likely delivered to and enriched in sediments in particulate form during temporally sporadic sulfidic events (Fig. 9a), though we cannot rule out reversal of porewater gradients during such events to permit downwards diffusion of Mo and U.

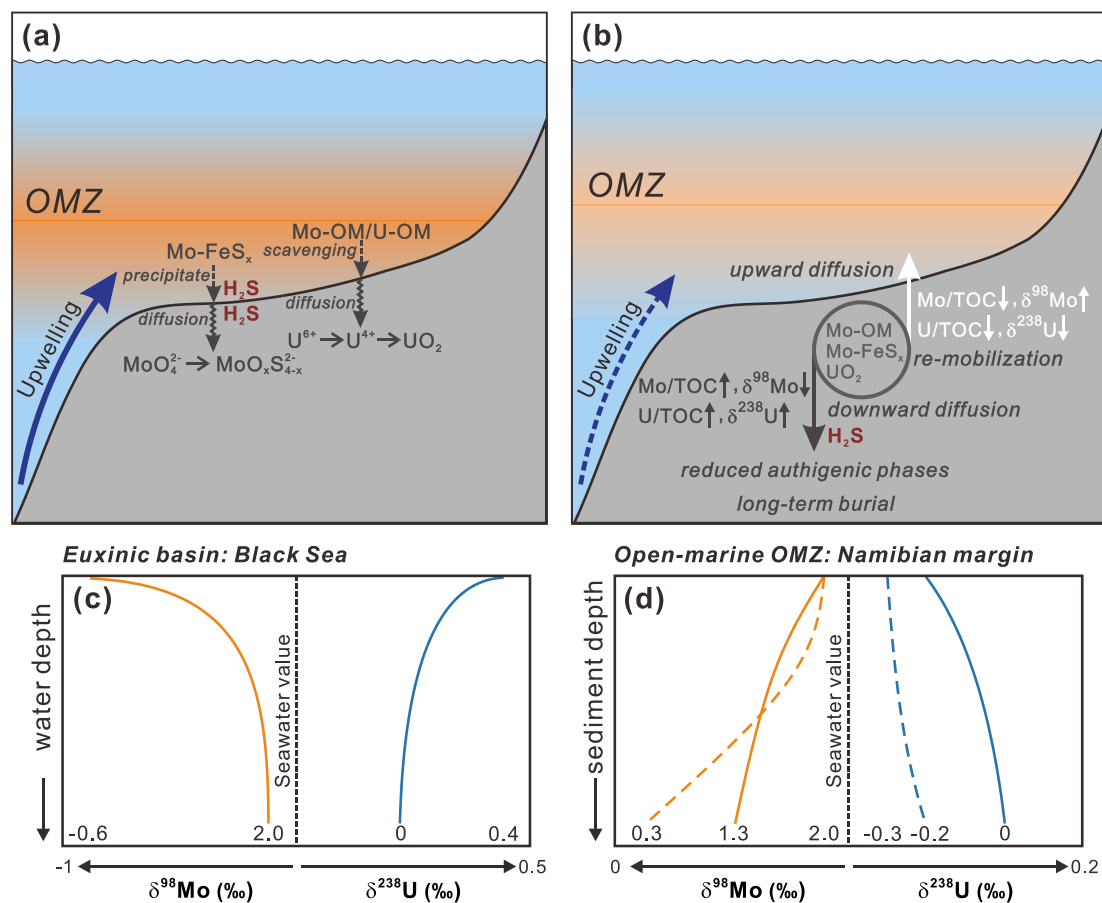


Fig. 9. (a and b) Schematic model illustrating Mo and U delivery and accumulation across the Namibian upwelling margin. (a) Sequestration of Mo and U from water column to sediment during intense productivity and reducing periods, via diffusion across the sediment–water interface with a potential role of scavenging to organic matter (Mo-OM and U-OM) or precipitation as Mo-Fe-S sulfides (Mo-FeS<sub>x</sub>) at the sediment–water interface. (b) Mo and U release from reduced solid phases followed by upward diffusion across the sediment–water interface and downward diffusion to the depth of removal. The diffusive re-distribution of Mo and U leads to high Mo/TOC, high U/TOC, low  $\delta^{98}\text{Mo}$ , and high  $\delta^{238}\text{U}$  in sediments at depth. (c and d) Schematic comparison of Mo and U isotope based paleoredox proxy signatures in (c) the euxinic Black Sea and (d) the open-marine OMZ (Namibian margin). (c) The solid curves depict water-depth dependence of authigenic  $\delta^{98}\text{Mo}$  and  $\delta^{238}\text{U}$  for the surface sediments in the Black Sea based on the data from Brüske et al. (2020). (d) The solid and dashed curves depict possible sediment-depth dependence of authigenic  $\delta^{98}\text{Mo}$  and  $\delta^{238}\text{U}$  based on the data for shelf and slope sediments from Namibian margin, respectively. See text for more details.

Both the porewater profiles and the patterns in authigenic Mo and U distribution with depth, suggest re-distribution of the Mo and U, sequestered to the sediment during temporally more reducing conditions, via oxidative dissolution under less reducing conditions and diffusion away from these local Mo and U porewater concentration peaks (Fig. 9b). Finally, the Mo and U are taken up again into reduced authigenic phases (sulfide-related) at depth, setting the final Mo and U isotope characteristics of the sediment (Fig. 9b).

Our findings also reveal that inverse correlations between authigenic Mo and U isotope signatures in sediments are not limited to semi-restricted euxinic settings, but may also occur in association with open-marine OMZs. A schematic comparison of the correlated Mo-U isotope systematics in the euxinic basin (Black Sea) and the open-marine OMZ (Namibian margin) is summarized in Fig. 9c and d. Because of the Black Sea's restricted character, the correlated Mo and U isotope signatures have been attributed to the changes in bottom-water sulfide concentrations and deep-water renewal rates (Fig. 9c). However, similar Mo-U isotope trends observed on the Namibian margin is the result of variability in diagenetic redox conditions (Fig. 9d), reflecting the impact of style of delivery and early diagenesis on Mo-U isotope compositions. In this light, the general coupling between Mo and U isotopes of the Namibian margin sediments provides a framework for the interpretation of such data in ancient open-marine settings.

#### Declaration of Competing Interest

The authors declare that they have no known competing financial interests or personal relationships that could have appeared to influence the work reported in this paper.

#### ACKNOWLEDGMENTS

We would like to thank the captain, the crew and the co-chief scientist Kurt Hanselmann, for their great work and support during the cruises on Namibia's R/V MIRABILIS. We also thank M. Jaggi, for help and support in the lab at ETH Zürich. ZWH acknowledges financial supports from the National Natural Science Foundation of China (41991324, 42006060), China Postdoctoral Science Foundation (2020M671201), the State Key Laboratory of Marine Geology (MG201905), and China Scholarship Council (201606340006). MOC and TCS were both funded by the EU's Horizon 2020 program under the Marie Skłodowska-Curie grant agreements 795722 and 834236, respectively. This study was also supported by funding from ETH Zürich and the Swiss National Science Foundation (SNF) through grant 200020-165904 to DV. We thank Florian Scholz and two anonymous reviewers for constructive comments that greatly improved this manuscript, and associate editor Brian Kendall for editorial handling.

#### APPENDIX A. SUPPLEMENTARY MATERIAL

Supplementary data to this article can be found online at <https://doi.org/10.1016/j.gca.2021.06.024>.

#### REFERENCES

- Abe M., Suzuki T., Fujii Y., Hada M. and Hirao K. (2008) An ab initio molecular orbital study of the nuclear volume effects in uranium isotope fractionations. *J. Chem. Phys.* **129**, 164309.
- Abshire M. L., Romaniello S. J., Kuzminov A. M., Cofrancesco J., Severmann S. and Riedinger N. (2020a) Uranium isotopes as a proxy for primary depositional redox conditions in organic-rich marine systems. *Earth Planet. Sci. Lett.* **529**, 115878.
- Abshire M. L., Owens J. D., Cofrancesco J., Inthorn M. and Riedinger N. (2020b) Geochemical signatures of redepositional environments: the Namibian continental margin. *Mari. Geol.* **429**, 106316.
- Algeo T. J. and Lyons T. W. (2006) Mo-total organic carbon covariation in modern anoxic marine environments: implications for analysis of paleoredox and paleohydrographic conditions. *Paleoceanography* **21**.
- Algeo T. J. and Tribovillard N. (2009) Environmental analysis of paleoceanographic systems based on molybdenum-uranium covariation. *Chem. Geol.* **268**, 211–225.
- Andersen M. B., Stirling C. H., Zimmermann B. and Halliday A. N. (2010) Precise determination of the open ocean  $^{234}\text{U}/^{238}\text{U}$  composition. *Geochem. Geophys. Geosyst.* **11**, Q12003.
- Andersen M. B., Romaniello S., Vance D., Little S. H., Herdman R. and Lyons T. W. (2014) A modern framework for the interpretation of  $^{238}\text{U}/^{235}\text{U}$  in studies of ancient ocean redox. *Earth Planet. Sci. Lett.* **400**, 184–194.
- Andersen M. B., Elliott T., Freymuth H., Sims K. W., Niu Y. and Kelley K. A. (2015) The terrestrial uranium isotope cycle. *Nature* **517**, 356–359.
- Andersen M., Vance D., Morford J., Bura-Nakić E., Breitenbach S. and Och L. (2016) Closing in on the marine  $^{238}\text{U}/^{235}\text{U}$  budget. *Chem. Geol.* **420**, 11–22.
- Andersen M. B., Stirling C. H. and Weyer S. (2017) Uranium isotope fractionation. *Rev. Mineral. Geochem.* **82**, 799–850.
- Andersen M. B., Matthews A., Vance D., Bar-Matthews M., Archer C. and de Souza G. F. (2018) A 10-fold decline in the deep Eastern Mediterranean thermohaline overturning circulation during the last interglacial period. *Earth Planet. Sci. Lett.* **503**, 58–67.
- Andersen M. B., Matthews A., Bar-Matthews M. and Vance D. (2020) Rapid onset of ocean anoxia shown by high U and low Mo isotope compositions of sapropel S1. *Geochem. Persp. Lett.* **15**, 10–14.
- Anderson R. F., Fleisher M. Q. and LeHuray A. P. (1989) Concentration, oxidation state, and particulate flux of uranium in the Black Sea. *Geochim. Cosmochim. Acta* **53**, 2215–2224.
- Archer C. and Vance D. (2008) The isotopic signature of the global riverine molybdenum flux and anoxia in the ancient oceans. *Nat. Geosci.* **1**, 597–600.
- Asael D., Tissot F. L., Reinhard C. T., Rouxel O., Dauphas N., Lyons T. W., Ponzevera E., Liorzou C. and Chéron S. (2013) Coupled molybdenum, iron and uranium stable isotopes as oceanic paleoredox proxies during the Paleoproterozoic Shunga Event. *Chem. Geol.* **362**, 193–210.
- Azrieli-Tal I., Matthews A., Bar-Matthews M., Almogi-Labin A., Vance D., Archer C. and Teutsch N. (2014) Evidence from molybdenum and iron isotopes and molybdenum-uranium covariation for sulphidic bottom waters during Eastern Mediterranean sapropel S1 formation. *Earth Planet. Sci. Lett.* **393**, 231–242.
- Barling J., Arnold G. L. and Anbar A. (2001) Natural mass-dependent variations in the isotopic composition of molybdenum. *Earth Planet. Sci. Lett.* **193**, 447–457.

- Barling J. and Anbar A. D. (2004) Molybdenum isotope fractionation during adsorption by manganese oxides. *Earth Planet. Sci. Lett.* **217**, 315–329.
- Böning P., Brumsack H.-J., Böttcher M. E., Schnetger B., Kriete C., Kallmeyer J. and Borchers S. L. (2004) Geochemistry of Peruvian near-surface sediments. *Geochim. Cosmochim. Acta* **68**, 4429–4451.
- Böning P., Schnetger B., Belz L., Ferdelman T., Brumsack H.-J. and Pahnke K. (2020) Sedimentary iron cycling in the Benguela upwelling system off Namibia. *Earth Planet. Sci. Lett.* **538**, 116212.
- Borchers S., Schnetger B., Böning P. and Brumsack H. J. (2005) Geochemical signatures of the Namibian diatom belt: Perennial upwelling and intermittent anoxia. *Geochem. Geophys. Geosyst.* **6**, Q06006.
- Bremner J. (1981) Shelf morphology and surficial sediment off central and northern South West Africa (Namibia). *Geo-Marine Lett.* **1**, 91.
- Brenneka G. A., Wasylenki L. E., Bargar J. R., Weyer S. and Anbar A. D. (2011) Uranium isotope fractionation during adsorption to Mn-oxyhydroxides. *Environ. Sci. Technol.* **45**, 1370–1375.
- Brüchert V., Jørgensen B. B., Neumann K., Riechmann D., Schlösser M. and Schulz H. (2003) Regulation of bacterial sulfate reduction and hydrogen sulfide fluxes in the central Namibian coastal upwelling zone. *Geochim. Cosmochim. Acta* **67**, 4505–4518.
- Brüchert V., Currie B., Peard K. R., Lass U., Endler R., Dübecke A., Julies E., Leipe T. and Zitzmann S. (2006) Biogeochemical and physical control on shelf anoxia and water column hydrogen sulphide in the Benguela coastal upwelling system off Namibia. In *Past and Present Water Column Anoxia* (ed. L. N. Neretin). Springer, pp. 161–193.
- Brüchert V., Currie B. and Peard K. R. (2009) Hydrogen sulphide and methane emissions on the central Namibian shelf. *Progr. Oceanogr.* **83**, 169–179.
- Brüske A., Weyer S., Zhao M. Y., Planavsky N. J., Wegwerth A., Neubert N., Dellwig O., Lau K. V. and Lyons T. W. (2020) Correlated molybdenum and uranium isotope signatures in modern anoxic sediments: implications for their use as paleoredox proxy. *Geochim. Cosmochim. Acta* **270**, 449–474.
- Bura-Nakić E., Andersen M. B., Archer C., de Souza G. F., Marguš M. and Vance D. (2018) Coupled Mo-U abundances and isotopes in a small marine euxinic basin: constraints on processes in euxinic basins. *Geochim. Cosmochim. Acta* **222**, 212–229.
- Calvert S. E. and Price N. B. (1983) Geochemistry of Namibian shelf sediments. In *Coastal Upwelling A. Its Sediment Record* (eds. E. Suess and J. Thiede). Plenum Press, pp. 337–369.
- Canfield D. E., Raiswell R., Westrich J. T., Reaves C. M. and Berner R. A. (1986) The use of chromium reduction in the analysis of reduced inorganic sulfur in sediments and shales. *Chem. Geol.* **54**, 149–155.
- Chen X., Ling H.-F., Vance D., Shields-Zhou G. A., Zhu M., Poulton S. W., Och L. M., Jiang S.-Y., Li D. and Cremonese L. (2015) Rise to modern levels of ocean oxygenation coincided with the Cambrian radiation of animals. *Nat. Commun.* **6**, 7.
- Cheng M., Li C., Zhou L., Algeo T. J., Zhang F., Romaniello S., Jin C.-S., Lei L.-D., Feng L.-J. and Jiang S.-Y. (2016) Marine Mo biogeochemistry in the context of dynamically euxinic mid-depth waters: a case study of the lower Cambrian Niutitang shales, South China. *Geochim. Cosmochim. Acta* **183**, 79–93.
- Cheng M., Li C., Jin C., Wang H., Algeo T. J., Lyons T. W., Zhang F. and Anbar A. (2020) Evidence for high organic carbon export to the early Cambrian seafloor. *Geochim. Cosmochim. Acta* **287**, 125–140.
- Clarkson M. O., Stirling C. H., Jenkyns H. C., Dickson A. J., Porcelli D., Moy C. M., von Strandmann P. A. P., Cooke I. R. and Lenton T. M. (2018) Uranium isotope evidence for two episodes of deoxygenation during Oceanic Anoxic Event 2. *Proc. Natl. Acad. Sci.* **115**, 2918–2923.
- Clarkson M. O., Müsing K., Andersen M. B. and Vance D. (2020) Examining pelagic carbonate-rich sediments as an archive for authigenic uranium and molybdenum isotopes using reductive cleaning and leaching experiments. *Chem. Geol.* **539**, 119412.
- Collier R. W. (1985) Molybdenum in the northeast Pacific Ocean. *Limnol. Oceanogr.* **30**, 1351–1354.
- Currie B., Utne-Palm A. C. and Salvanes A. G. V. (2018) Winning ways with hydrogen sulphide on the Namibian Shelf. *Front. Mar. Sci.* **5**, 341.
- Dahl T. W., Chappaz A., Hoek J., McKenzie C. J., Svane S. and Canfield D. E. (2017) Evidence of molybdenum association with particulate organic matter under sulfidic conditions. *Geobiology* **15**, 311–323.
- Dickson A. J., Cohen A. S. and Coe A. L. (2014) Continental margin molybdenum isotope signatures from the early Eocene. *Earth. Planet. Sci. Lett.* **404**, 389–395.
- Dickson A. J. (2017) A molybdenum-isotope perspective on Phanerozoic deoxygenation events. *Nat. Geosci.* **10**, 721–726.
- Dunk R., Mills R. and Jenkins W. (2002) A reevaluation of the oceanic uranium budget for the Holocene. *Chem. Geol.* **190**, 45–67.
- Emeis K.-C., Brüchert V., Currie B., Endler R., Ferdelman T., Kiessling A., Leipe T., Noli-Peard K., Struck U. and Vogt T. (2004) Shallow gas in shelf sediments of the Namibian coastal upwelling ecosystem. *Continental Shelf Res.* **24**, 627–642.
- Erickson B. E. and Helz G. R. (2000) Molybdenum (VI) speciation in sulfidic waters: stability and lability of thiomolybdates. *Geochim. Cosmochim. Acta* **64**, 1149–1158.
- Eroglu S., Scholz F., Frank M. and Siebert C. (2020) Influence of particulate versus diffusive molybdenum supply mechanisms on the molybdenum isotope composition of continental margin sediments. *Geochim. Cosmochim. Acta* **273**, 51–69.
- Fossing H., Ferdelman T. G. and Berg P. (2000) Sulfate reduction and methane oxidation in continental margin sediments influenced by irrigation (South-East Atlantic off Namibia). *Geochim. Cosmochim. Acta* **64**, 897–910.
- Goldberg T., Archer C., Vance D. and Poulton S. W. (2009) Mo isotope fractionation during adsorption to Fe (oxyhydr)oxides. *Geochim. Cosmochim. Acta* **73**, 6502–6516.
- Goldberg T., Archer C., Vance D., Thamdrup B., McAnena A. and Poulton S. W. (2012) Controls on Mo isotope fractionations in a Mn-rich anoxic marine sediment, Gullmar Fjord, Sweden. *Chem. Geol.* **296**, 73–82.
- Helz G., Miller C., Charnock J., Mosselmans J., Pattrick R., Garner C. and Vaughan D. (1996) Mechanism of molybdenum removal from the sea and its concentration in black shales: EXAFS evidence. *Geochim. Cosmochim. Acta* **60**, 3631–3642.
- Helz G. R., Bura-Nakić E., Mikac N. and Ciglencečki I. (2011) New model for molybdenum behavior in euxinic waters. *Chem. Geol.* **284**, 323–332.
- Hinojosa J. L., Stirling C. H., Reid M. R., Moy C. M. and Wilson G. S. (2016) Trace metal cycling and <sup>238</sup>U/<sup>235</sup>U in New Zealand's fjords: implications for reconstructing global paleoredox conditions in organic-rich sediments. *Geochim. Cosmochim. Acta* **179**, 89–109.
- Holmden C., Amini M. and Francois R. (2015) Uranium isotope fractionation in Saanich Inlet: a modern analog study of a paleoredox tracer. *Geochim. Cosmochim. Acta* **153**, 202–215.
- Hutchings A. M., Basu A., Dickson A. J. and Turchyn A. V. (2020) Molybdenum Geochemistry in Salt Marsh Pond Sediments. *Geochim. Cosmochim. Acta* **284**, 75–91.

- Inthorn M., Mohrholz V. and Zabel M. (2006a) Nepheloid layer distribution in the Benguela upwelling area offshore Namibia. *Deep-Sea Res. I* **53**, 1423–1438.
- Inthorn M., Wagner T., Scheeder G. and Zabel M. (2006b) Lateral transport controls distribution, quality, and burial of organic matter along continental slopes in high-productivity areas. *Geology* **34**, 205–208.
- Kendall B., Gordon G. W., Poulton S. W. and Anbar A. D. (2011) Molybdenum isotope constraints on the extent of late Paleoproterozoic ocean euxinia. *Earth Planet. Sci. Lett.* **307**, 450–460.
- Kendall B., Komiya T., Lyons T. W., Bates S. M., Gordon G. W., Romaniello S. J., Jiang G., Creaser R. A., Xiao S. and McFadden K. (2015) Uranium and molybdenum isotope evidence for an episode of widespread ocean oxygenation during the late Ediacaran Period. *Geochim. Cosmochim. Acta* **156**, 173–193.
- Kendall B., Dahl T. W. and Anbar A. D. (2017) The stable isotope geochemistry of molybdenum. *Rev. Mineral. Geochem.* **82**, 683–732.
- Kendall B., Wang J., Zheng W., Romaniello S. J., Jeffrey Over D., Bennett Y., Xing L., Kunert A., Boyes C. and Liu J. (2020) Inverse correlation between the molybdenum and uranium isotope compositions of Upper Devonian black shales caused by changes in local depositional conditions rather than global ocean redox variations. *Geochim. Cosmochim. Acta* **287**, 141–164.
- Kerl C. F., Lohmayer R., Bura-Nakic´ E., Vance D. and Planer-Friedrich B. (2017) Experimental confirmation of isotope fractionation in thiomolybdates using ion chromatographic separation and detection by multicollector ICPMS. *Anal. Chem.* **89**, 3123–3129.
- Lau K. V., Lyons T. W. and Maher K. (2020) Uranium reduction and isotopic fractionation in reducing sediments: Insights from reactive transport modeling. *Geochim. Cosmochim. Acta*.
- Lovley D. R., Phillips E. J. P., Gorby Y. A. and Landa E. R. (1991) Microbial reduction of uranium. *Nature* **350**, 413–416.
- Lu X., Dahl T. W., Zheng W., Wang S. and Kendall B. (2020) Estimating ancient seawater isotope compositions and global ocean redox conditions by coupling the molybdenum and uranium isotope systems of euxinic organic-rich mudrocks. *Geochim. Cosmochim. Acta* **290**, 76–103.
- Manheim F. and Lane-Bostwick C. (1991) Chemical composition of ferromanganese crusts in the world ocean: a review and comprehensive database. Open-File Report 89–020, US Geological Survey, Woods Hole, MA.
- Matthews A., Azrieli-Tal I., Benkovitz A., Bar-Matthews M., Vance D., Poulton S. W., Teutsch N., Almogi-Labin A. and Archer C. (2017) Anoxic development of sapropel S1 in the Nile Fan inferred from redox sensitive proxies, Fe speciation, Fe and Mo isotopes. *Chem. Geol.* **475**, 24–39.
- McLennan S. M. (2001) Relationships between the trace element composition of sedimentary rocks and upper continental crust. *Geochem. Geophys. Geosyst.* **2**, 2000GC000109.
- McManus J., Berelson W. M., Severmann S., Poulson R. L., Hammond D. E., Klinkhammer G. P. and Holm C. (2006) Molybdenum and uranium geochemistry in continental margin sediments: paleoproxy potential. *Geochim. Cosmochim. Acta* **70**, 4643–4662.
- Miller C. A., Peucker-Ehrenbrink B., Walker B. D. and Marcantonio F. (2011) Re-assessing the surface cycling of molybdenum and rhenium. *Geochim. Cosmochim. Acta* **75**, 7146–7179.
- Mohrholz V., Bartholomae C. H., van der Plas A. K. and Lass H. U. (2008) The seasonal variability of the northern Benguela undercurrent and its relation to the oxygen budget on the shelf. *Cont. Shelf Res.* **28**, 424–441.
- Mollenhauer G., Schneider R. R., Müller P. J., Spieß V. and Wefer G. (2002) Glacial/inter-glacial variability in the Benguela upwelling system: spatial distribution and budgets of organic carbon accumulation. *Glob. Biogeochem. Cycles* **16**, 1134.
- Monteiro P. M. S., van der Plas A., Mohrholz V., Mabilley E., Pascall A. and Joubert W. (2006) Variability of natural hypoxia and methane in a coastal upwelling system: Oceanic physics or shelf biology? *Geophys. Res. Lett.* **33**, L16614.
- Morford J. L. and Emerson S. (1999) The geochemistry of redox sensitive trace metals in sediments. *Geochim. Cosmochim. Acta* **63**, 1735–1750.
- Morford J. L., Martin W. R., Kalnejais L. H., François R., Bothner M. and Karle I.-M. (2007) Insights on geochemical cycling of U, Re and Mo from seasonal sampling in Boston Harbor, Massachusetts, USA. *Geochim. Cosmochim. Acta* **71**, 895–917.
- Nagel B., Emeis K.-C., Flohr A., Rixen T., Schlarbaum T., Mohrholz V. and van der Plas A. (2013) N-cycling and balancing of the N-deficit generated in the oxygen minimum zone over the Namibian shelf—an isotope-based approach. *J. Geophys. Res. Biogeosci.* **118**, 361–371.
- Nägler T. F., Siebert C., Lüschen H. and Böttcher M. E. (2005) Sedimentary Mo isotope record across the Holocene fresh-brackish water transition of the Black Sea. *Chem. Geol.* **219**, 283–295.
- Nägler T. F., Anbar A. D., Archer C., Goldberg T., Gordon G. W., Greber N. D., Siebert C., Sohrin Y. and Vance D. (2014) Proposal for an international molybdenum isotope measurement standard and data representation. *Geostand. Geoanal. Res.* **38**, 149–151.
- Nakagawa Y., Takano S., Firdaus M. L., Norisuye K., Hirata T., Vance D. and Sohrin Y. (2012) The molybdenum isotopic composition of the modern ocean. *Geochem. J.* **46**, 131–141.
- Nelson G. and Hutchings L. (1983) The Benguela upwelling area. *Prog. Oceanogr.* **12**, 333–356.
- Neubert N., Nægler T. F. and Böttcher M. E. (2008) Sulfidity controls molybdenum isotope fractionation into euxinic sediments: Evidence from the modern Black Sea. *Geology* **36**, 775–778.
- Noordmann J., Weyer S., Montoya-Pino C., Dellwig O., Neubert N., Eckert S., Paetzel M. and Böttcher M. E. (2015) Uranium and molybdenum isotope systematics in modern euxinic basins: Case studies from the central Baltic Sea and the Kyllaren fjord (Norway). *Chem. Geol.* **396**, 182–195.
- Ohde T., Siegel H., Reißmann J. and Gerth M. (2007) Identification and investigation of sulphur plumes along the Namibian coast using the MERIS sensor. *Cont. Shelf Res.* **27**, 744–756.
- Ohde T. and Dadou I. (2018) Seasonal and annual variability of coastal sulphur plumes in the northern Benguela upwelling system. *PLoS ONE* **13** e0192140.
- Poulson Brucker R. L., McManus J., Severmann S. and Berelson W. M. (2009) Molybdenum behavior during early diagenesis: insights from Mo isotopes. *Geochem. Geophys. Geosyst.* **10**.
- Richter S., Alonso-Munoz A., Eykens R., Jacobsson U., Kuehn H., Verbruggen A., Aregbe Y., Wellum R. and Keegan E. (2008) The isotopic composition of natural uranium samples—measurements using the new  $n(^{233}\text{U})/n(^{236}\text{U})$  double spike IRMM-3636. *Int. J. Mass Spectrom.* **269**, 145–148.
- Rolison J. M., Stirling C. H., Middag R. and Rijkenberg M. J. (2017) Uranium stable isotope fractionation in the Black Sea: modern calibration of the  $^{238}\text{U}/^{235}\text{U}$  paleo-redox proxy. *Geochim. Cosmochim. Acta* **203**, 69–88.
- Schauble E. A. (2007) Role of nuclear volume in driving equilibrium stable isotope fractionation of mercury, thallium, and other very heavy elements. *Geochim. Cosmochim. Acta* **71**, 2170–2189.

- Scholz F., Hensen C., Noffke A., Rohde A., Liebetrau V. and Wallmann K. (2011) Early diagenesis of redox-sensitive trace metals in the Peru upwelling area – response to ENSO-related oxygen fluctuations in the water column. *Geochim. Cosmochim. Acta* **75**, 7257–7276.
- Scholz F., Severmann S., McManus J., Noffke A., Lomnitz U. and Hensen C. (2014) On the isotope composition of reactive iron in marine sediments: redox shuttle versus early diagenesis. *Chem. Geol.* **389**, 48–59.
- Scholz F., Siebert C., Dale A. W. and Frank M. (2017) Intense molybdenum accumulation in sediments underneath a nitrogenous water column and implications for the reconstruction of paleo-redox conditions based on molybdenum isotopes. *Geochim. Cosmochim. Acta* **213**, 400–417.
- Scholz F., Baum M., Siebert C., Eroglu S., Dale A. W., Naumann M. and Sommer S. (2018) Sedimentary molybdenum cycling in the aftermath of seawater inflow to the intermittently euxinic Gotland Deep, Central Baltic Sea. *Chem. Geol.* **491**, 27–38.
- Seeberg-Elverfeldt J., Schlüter M., Feseker T. and Kölling M. (2005) Rhizon sampling of porewaters near the sediment-water interface of aquatic systems. *Limnol. Oceanogr.: Methods* **3**, 361–371.
- Shannon L. V. (1985) The Benguela Ecosystem: 1. evolution of the Benguela, physical features and processes. *Oceanogr. Mar. Biol.* **23**, 105–182.
- Shannon L. V. and Nelson G. (1996) The Benguela: large scale features and processes and system variability. In *The South Atlantic: Present and Past Circulation* (eds. G. Wefer, W. H. Berger, G. Siedler and D. J. Webb). Springer, Berlin, Heidelberg, pp. 163–210.
- Stockey R. G., Cole D. B., Planavsky N. J., Loydell D. K., Frýda J. and Sperling E. A. (2020) Persistent global marine euxinia in the early Silurian. *Nat. Commun.* **11**, 1804.
- Stramma L. and England S. (1999) On the water masses and mean circulation of the South Atlantic Ocean. *J. Geophys. Res.* **104**, 20863–20883.
- Shaw T. J., Gieskes J. M. and Jahnke R. A. (1990) Early diagenesis in differing depositional environments: the response of transition metals in pore water. *Geochim. Cosmochim. Acta* **54**, 1233–1246.
- Siebert C., Nägler T. F., von Blanckenburg F. and Kramers J. D. (2003) Molybdenum isotope records as a potential new proxy for paleoceanography. *Earth Planet. Sci. Lett.* **211**, 159–171.
- Siebert C., McManus J., Bice A., Poulson R. and Berelson W. M. (2006) Molybdenum isotope signatures in continental margin marine sediments. *Earth Planet. Sci. Lett.* **241**, 723–733.
- Stirling C. H., Andersen M. B., Potter E.-K. and Halliday A. N. (2007) Low-temperature isotopic fractionation of uranium. *Earth Planet. Sci. Lett.* **264**, 208–225.
- Tissot F. L. and Dauphas N. (2015) Uranium isotopic compositions of the crust and ocean: age corrections, U budget and global extent of modern anoxia. *Geochim. Cosmochim. Acta* **167**, 113–143.
- Tossell J. (2005) Calculating the partitioning of the isotopes of Mo between oxidic and sulfidic species in aqueous solution. *Geochim. Cosmochim. Acta* **69**, 2981–2993.
- Tostevin R., Clarkson M. O., Gangl S., Shields G. A., Wood R. A., Bowyer F., Penny A. M. and Stirling C. H. (2019) Uranium isotope evidence for an expansion of anoxia in terminal Ediacaran oceans. *Earth Planet. Sci. Lett.* **506**, 104–112.
- Tribouillard N., Algeo T. J., Lyons T. and Riboulleau A. (2006) Trace metals as paleoredox and paleoproductivity proxies: an update. *Chem. Geol.* **232**, 12–32.
- Voegelin A. R., Pettke T., Greber N. D., von Niederhäusern B. and Nägler T. F. (2014) Magma differentiation fractionates Mo isotope ratios: evidence from the Kos Plateau Tuff (Aegean Arc). *Lithos* **190**, 440–448.
- Wang X., Planavsky N. J., Reinhard C. T., Hein J. R. and Johnson T. M. (2016) A Cenozoic seawater redox record derived from  $^{238}\text{U}/^{235}\text{U}$  in ferromanganese crusts. *Am. J. Sci.* **316**, 64–83.
- Wasylenki L. E., Rolfe B. A., Weeks C. L., Spiro T. G. and Anbar A. D. (2008) Experimental investigation of the effects of temperature and ionic strength on Mo isotope fractionation during adsorption to manganese oxides. *Geochim. Cosmochim. Acta* **72**, 5997–6005.
- Weeks S. J., Currie B. and Bakun A. (2002) Massive emissions of toxic gas in the Atlantic. *Nature* **415**, 493–494.
- Weeks S. J., Currie B., Bakun A. and Peard K. R. (2004) Hydrogen sulphide eruptions in the Atlantic Ocean off southern Africa: implications of a new view based on SeaWiFS satellite imagery. *Deep-Sea Res. Part I* **51**, 153–172.
- Weyer S., Anbar A., Gerdes A., Gordon G., Algeo T. and Boyle E. (2008) Natural fractionation of  $^{238}\text{U}/^{235}\text{U}$ . *Geochim. Cosmochim. Acta* **72**, 345–359.
- Zhang F., Dahl T. W., Lenton T. M., Luo G., Shen S.-Z., Algeo T. J., Planavsky N., Liu J., Cui Y., Qie W., Romaniello S. J. and Anbar A. D. (2020) Extensive marine anoxia associated with the Late Devonian Hangenberg Crisis. *Earth Planet. Sci. Lett.* **533**, 115976.
- Zheng Y., Anderson R. F., van Geen A. and Kuwabara J. (2000) Authigenic molybdenum formation in marine sediments: a link to pore water sulfide in the Santa Barbara Basin. *Geochim. Cosmochim. Acta* **64**, 4165–4178.
- Zheng Y., Anderson R. F., Van Geen A. and Fleisher M. Q. (2002) Remobilization of authigenic uranium in marine sediments by bioturbation. *Geochim. Cosmochim. Acta* **66**, 1759–1772.

Associate editor: Brian Kendall